

Gain and index guiding effects in an injection seeded Raman amplifier
by Kevin Scot Repasky

A thesis submitted in partial fulfillment of the requirements for the degree of Doctor of Philosophy in Physics
Montana State University
© Copyright by Kevin Scot Repasky (1996)

Abstract:
A theory is presented for an injection seeded Raman amplifier which includes the total Raman susceptibility. Calculations indicate that the imaginary part of the Raman susceptibility leads to gain and gain guiding while the real part of the Raman susceptibility leads to index guiding. Both the gain and index guiding affect the spatial structure of the amplified Stokes beam. When the input Stokes beam is tuned to the blue (red) side of the Raman resonance, the amplified Stokes beam is focused (defocused) due to the real part of the Raman susceptibility. The calculations also indicate the peak Stokes output from the Raman amplifier occurs when the input Stokes is tuned to the blue side of the Raman resonance. Experimental results are presented that measure the amplified Stokes beam's spatial structure. The results from this experiment confirm the prediction of a narrower (wider) Stokes beam when the input Stokes is tuned to the blue (red) side of the Raman resonance. The narrower amplified Stokes beam when the input Stokes is tuned to the blue side of the Raman resonance results in the amplified Stokes beam experiencing an increased gain. This increased gain that occurs on the blue side of the Raman resonance is confirmed by an experiment.

GAIN AND INDEX GUIDING EFFECTS IN AN INJECTION SEEDED RAMAN AMPLIFIER

by

Kevin Scot Repasky

A thesis submitted in partial fulfillment
of the requirements for the degree

of

Doctor of Philosophy

in

Physics

MONTANA STATE UNIVERSITY
Bozeman, Montana

December 1996

D378
R299

APPROVAL

of a thesis submitted by

Kevin Scot Repasky

This thesis has been read by each member of the thesis committee and has been found to be satisfactory regarding content, English usage, format, citations, bibliographic style, and consistency, and is ready for submission to the College of Graduate Studies.

John L. Carlsten — Chairperson, Graduate Committee — Date: 1-13-97

Approved for the Department of Physics

John Hermanson — Head, Major Department — Date: 1-13-97

Approved for the College of Graduate Studies

Graduate Dean — Date: 1/20/97

STATEMENT OF PERMISSION TO USE

In presenting this thesis in partial fulfillment of the requirements for a doctoral degree at Montana State University-Bozeman, I agree that the Library shall make it available to borrowers under rules of the Library. I further agree that copying of this thesis is allowed only for scholarly purposes, consistent with "fair use" as prescribed in the U.S. Copyright Law. Requests for extensive copying or reproduction of this thesis should be referred to University Microfilms International, 300 North Zeeb Road, Ann Arbor, Michigan 48106, to whom I have granted "the exclusive right to reproduce and distribute my dissertation in and from microform along with the non-exclusive right to reproduce and distribute my abstract in any format in whole or in part."

Signature Kevin Repasky

Date 1-13-97

ACKNOWLEDGMENTS

First and foremost, I would like to thank my advisor, John Carlsten, for giving me the opportunity to work in his lab. His infinite patience and encouragement has made my tenure in his lab a most rewarding experience.

I would like to thank the many people who I have had the pleasure to work with. Thanks are due to Jim Wessel who helped me get started in the lab. We had many great times, laughs, and late nights. Also, thanks are due to Jay Brasseur for help on the latest experiments. Also, thanks go to Gregg Switzer, Meg Hall and the numerous undergraduates who have worked in the lab.

I am grateful to my graduate committee for reading my thesis. I have incorporated many of their suggested changes into this thesis.

I would like to thank Erik Anderson and Norm Williams for their help with electronics and machining.

I would like to thank my mom for encouraging me to chase my dreams. Also thanks go to Dr. and Mrs. Ketcham for all their help that I will never be able to repay.

Finally, thanks go to my wife Terry Rick who has supported me throughout.

TABLE OF CONTENTS

		Page
1.	INTRODUCTION	1
	Raman Scattering	1
	Background	3
	Gain and Index Guiding	4
2.	THE WAVE EQUATION AND METHOD OF SOLUTION	11
	Introduction	11
	Wave Equation	12
	The Nonlinear Raman Susceptibility	13
	Approximate Solution to the Wave Equation	14
	Solution to the Wave Equation	17
	The Gauss-Laguerre Basis	18
	The Nonorthogonal Basis	22
3.	MODE STRUCTURE OF THE AMPLIFIED STOKES FIELD	27
	Introduction	27
	Physical Arguments for Gain and Index Guiding	28
	Mode Structure of the Amplified Stokes Field	29
	Enhanced Performance of a Raman Amplifier	33
4.	SEEDING OF A RAMAN AMPLIFIER WITH A VISIBLE LASER DIODE	45
	Introduction	45
	Experiment	46
	High Finesse Interferometers	48
	Results	52
5.	SPATIAL STRUCTURE OF THE AMPLIFIED STOKES FIELD	60
	Introduction	60
	Spatial Structure Experiment	61
	Results	64
6.	FREQUENCY ASYMMETRIC GAIN PROFILE IN A SEEDED RAMAN AMPLIFIER	73
	Introduction	73

TABLE OF CONTENTS - Continued

	Frequency Dependence of the Stokes Output	74
	Experiment	77
	Experimental Results	78
7.	CONCLUSION	86
	Summary	86
	Future	88
	REFERENCES CITED	89
	APPENDICES	94
A.	The Wave Equation	95
B.	Transient Stimulated Raman Scattering Equations	98
C.	The Nonlinear Raman Susceptibility	101
D.	The Gauss-Laguerre Modes	107
E.	The $A^{l}_{p',p}(\mu, G; \theta, \theta_m)$ Matrix Elements	114
F.	Mode Matching and Alignment of the High Finesse Interferometer	117
G.	Raman Linewidth	124

LIST OF FIGURES

Figure		Page
1.	Energy level diagram	9
2.	Simplified experimental setup	10
3.	Gain guiding	36
4.	Phasefronts affected by a lens	37
5.	Phasefronts for zero detuning	38
6.	Spatial profile for zero detuning	39
7.	Phasefronts for detuning to the blue side of the Raman resonance	40
8.	Phasefronts for detuning to the red side of the Raman resonance	41
9.	Spatial profiles including detuning	42
10.	Phasefronts including modified input	43
11.	Enhanced performance for modified input	44
12.	Experimental setup for seeding experiment	55
13.	Schematic of the high finesse interferometer	56
14.	Raw data for seeding experiment	57
15.	Sorted data for seeding experiment	58
16.	Output Stokes energy as a function of pump energy	59
17.	Experimental setup for spatial structure experiment	68
18.	Theoretical prediction for the spatial structure as a function of detuning	69
19.	Real part of the Raman susceptibility	70
20.	Normalized Stokes energy as a function of detuning	71
21.	Experimental results for the spatial structure	72
22.	Normalized Stokes energy as a function of detuning and gain	80
23.	Raman linewidth	81
24.	Detuning that maximizes Stokes output as a function of gain	82
25.	Experimental setup for asymmetric gain experiment	83
26.	Stokes output as a function of seed frequency	84
27.	Experimental detuning that maximizes the Stokes output as a function of gain	85
D1.	The U_0^0 Gauss-Laguerre mode	110
D2.	The U_2^0 Gauss-Laguerre mode	111
D3.	The U_0^2 Gauss-Laguerre mode	112
D4.	The U_2^2 Gauss-Laguerre mode	113
F1.	Experimental setup for mode matching	121
F2.	Experimental apparatus to align the HFI	122
F3.	Video image and oscilloscope trace at various stages of mode matching	123
G1.	Raman linewidth as a function of pressure	127

ABSTRACT

A theory is presented for an injection seeded Raman amplifier which includes the total Raman susceptibility. Calculations indicate that the imaginary part of the Raman susceptibility leads to gain and gain guiding while the real part of the Raman susceptibility leads to index guiding. Both the gain and index guiding affect the spatial structure of the amplified Stokes beam. When the input Stokes beam is tuned to the blue (red) side of the Raman resonance, the amplified Stokes beam is focused (defocused) due to the real part of the Raman susceptibility. The calculations also indicate the peak Stokes output from the Raman amplifier occurs when the input Stokes is tuned to the blue side of the Raman resonance. Experimental results are presented that measure the amplified Stokes beam's spatial structure. The results from this experiment confirm the prediction of a narrower (wider) Stokes beam when the input Stokes is tuned to the blue (red) side of the Raman resonance. The narrower amplified Stokes beam when the input Stokes is tuned to the blue side of the Raman resonance results in the amplified Stokes beam experiencing an increased gain. This increased gain that occurs on the blue side of the Raman resonance is confirmed by an experiment.

CHAPTER 1

INTRODUCTION

Raman Scattering

Raman scattering[1-3] is an inelastic scattering process in which a photon is scattered off a Raman active medium. Because the scattering process is inelastic, the scattered photon can either deposit some of its energy in the Raman active medium which results in a red shifted scattered photon or extract some energy from the Raman active medium which results in a blue shifted scattered photon. The red shifted scattered photon is often referred to as a Stokes photon while the blue shifted scattered photon is referred to as an antiStokes photon.

A schematic energy level diagram for a typical Raman scattering process is shown in Fig.1. The energy level labeled $|1\rangle$ is the ground state of the Raman active medium, the energy level labeled $|2\rangle$ is usually the first excited electronic state, and the energy level labeled $|3\rangle$ can result from a vibrational or rotational excited state of the Raman active medium. A pump photon with energy $\hbar\omega_p$, where ω_p is the frequency of the

pump photon, is scattered off the Raman active medium leaving the Raman active medium in the excited state $|3\rangle$. The energy of the scattered photon can be found from conservation of energy to be $\hbar\omega_s = \hbar\omega_p - \hbar\omega_{13}$ where $\hbar\omega_{13}$ corresponds to the energy difference between levels $|1\rangle$ and $|3\rangle$ shown in Fig.1 and ω_s is the frequency of the scattered photon. The frequency of the scattered photon has been red shifted and the scattered photon is referred to as a Stokes photon.

Scattering can occur either by spontaneous scattering or stimulated scattering. Spontaneous scattering occurs when just a pump photon is incident on the Raman active medium. A single Stokes photon is created at the frequency ω_s after the scattering event has occurred. Stimulated Raman scattering occurs when both a pump photon at the frequency ω_p and an input Stokes photon at ω_s are incident on the Raman active medium. Two Stokes photons at the frequency ω_s come out after the scattering event. In the case of stimulated Raman scattering, the input Stokes photon is amplified by the scattering event.

A simplified schematic of an experiment which studies stimulated Raman scattering is shown in Fig.2. A high power laser provides a source of pump photons for the stimulated Raman scattering. Input Stokes photons can be generated for example by spontaneous emission or by a tunable laser diode centered at the frequency ω_s. The input Stokes photons are combined at the beam combiner with the pump photons and sent colinearly through a Raman active medium. The amplified Stokes and residual pump are separated by a dispersive element such as a prism.

The Raman active medium used for all the work in this thesis is diatomic hydrogen. The H_2 is contained in a cell at high pressures. The state labeled $|1\rangle$ in Fig.1 is the ground state of the H_2 molecule while the state labeled $|2\rangle$ is the first excited electronic state and is 11.2eV above the ground state. The state labeled $|3\rangle$ is the first excited vibrational state and is 0.51ev above the ground state. The source of pump photons in the experiments to be discussed in this thesis come from a frequency doubled Nd:YAG laser at a wavelength of λ_p=532nm which corresponds to an energy for the pump photon of 2.33eV. The scattered Stokes photons are at a wavelength of λ_s=683nm which corresponds to an energy for the scattered Stokes photon of 1.82eV.

Background

Laser induced Raman scattering was first studied in 1962[4] and ever since has provided a productive area for research. Raman scattering is used in spectroscopic systems[3,5] where the frequency shift of the scattered light, which is characteristic of the scattering medium, is used to identify the scatterer. Raman scattering is also used as a way to shift frequencies of lasers by integer multiples of the frequency ω_{13} [6,7] (shown in Fig.1). More recently, Raman scattering has been used to study temporal solitons[8-14]. It was found that the Raman solitons occur spontaneously and the origin of this phenomena is a result of quantum fluctuations[8,14]. The quantum fluctuations or quantum noise were shown to be at the one photon per mode noise limit for a phase insensitive optical amplifier[15,16]. The noise limit of one photon per mode implies that the quantum noise can

easily be dominated in a Raman amplifier by using an input Stokes signal of only a few photons.

More recently, work has focused on looking at the full three dimensional aspect of the Raman amplifier.. The focused nature of the pump beam and transverse variations in the gain are taken into account in a theory which utilizes a nonorthogonal modal basis expansion to describe the amplified Stokes field[17-22]. The initial nonorthogonal modal theory describes the energy output of the Raman amplifier[19] but fails to correctly predict the spatial structure of the amplified Stokes output. Modifying the wave equation to include the effects of index guiding and using a similar nonorthogonal modal expansion to describe the amplified field correctly predicts the measured spatial structure of the amplified Stokes output[23]. Including the effects of index guiding also leads to the unintuative prediction that the peak Stokes output does not occur when the input Stokes signal is tuned to the Raman resonance but rather occurs when the input Stokes signal is tuned to the blue side of the Raman resonance[24]. Investigating the index guiding effects in a Raman amplifier is the main thrust of this thesis.

Gain and Index Guiding

Gain[19,20,25] and index[23,24,26] guiding are two effects which influence the spatial structure of the amplified Stokes beam as it grows in a Raman amplifier. In fact, gain and index guiding will occur whenever a gain profile that is nonuniform in the transverse

direction is present. The work done in this thesis with Raman amplifiers will carry over into many other types of optical amplifiers.

Gain guiding, as the name implies, is related to the gain of an amplifier. The origin of the gain in the Raman amplifier can be traced back to the imaginary part of the Raman susceptibility[1]. Most theories which have described Raman amplifiers to this point have only included the imaginary term of the Raman susceptibility[8-22]. However, the Kramers-Kronig relationship[1] tells us that if we have an imaginary part of the Raman susceptibility then we must also have a real part of the Raman susceptibility. The real part of the Raman susceptibility affects the index of refraction[1] that the amplified Stokes beam experiences and leads to index guiding. Because the real and imaginary parts of the Raman susceptibility are intertwined by the Kramers-Kronig relationships, gain and index guiding are intertwined and their effects must be studied together.

Gain guiding affects the spatial structure of the amplified Stokes beam as follows. The gain profile in a Raman amplifier is proportional to the pump laser intensity and has a gaussian profile. The input Stokes grows faster at the center of the gain profile where the gain is larger than at the wings. Because the center of the Stokes beam grows more rapidly than the wings, the amplified Stokes beam narrows.

Index guiding also affects the structure of the Stokes beam and acts as follows. The real part of the Raman susceptibility leads to an index of refraction which has a nonuniform transverse profile. A lens can be modeled by a nonuniform transverse index

of refraction. Therefore, we can say that the real part of the Raman susceptibility creates an effective lens which will change the spatial structure of the amplified Stokes beam.

To understand the spatial structure of the amplified Stokes beam, the Raman susceptibility must be included in the wave equation that describes the Raman amplifier. No noise term will be included in this wave equation since we are modeling an injection seeded Raman amplifier where the input Stokes signal is large enough to dominate the effects of quantum noise.

The wave equation is solved in chapter 2 by two different methods. The first method involves expanding the amplified Stokes field over the Gauss-Laguerre basis[27,28]. The Gauss-Laguerre basis turns out to be a nice basis to work with because the input Stokes field is a focused gaussian and can be described by only the lowest order Gauss-Laguerre mode. The input mode is coupled to several modes in the Raman amplifier via the Raman gain and this allows the output of the Raman amplifier to have a different spatial structure than the input Stokes signal. The output of the Raman amplifier however is described by many modes and this makes the Gauss-Laguerre basis awkward for describing the output of the Raman amplifier. The second method of solution which will also be presented in chapter 2 involves expanding the amplified Stokes field over a nonorthogonal modal basis[17-22]. The nonorthogonal modal basis is a natural modal basis for describing the output of the Raman amplifier. In the high gain limit, the amplified output Stokes field can be described by a single nonorthogonal mode[19]. However, the

input to the Raman amplifier which is a focused gaussian must now be expanded over the more complicated nonorthogonal modes.

The numerical results from solving the wave equation are presented in chapter 3. The effects of gain and index guiding on the spatial structure including the phasefronts are studied in this chapter. Surprisingly, the numerical results indicate that tuning the input Stokes signal to the blue side of Raman resonance can be used to increase the output of the Raman amplifier. A brief discussion on improving the performance of the Raman amplifier by modifmg the phasefronts of the input Stokes beam to better overlap the phasefronts supported by th Raman amplifier is presented.

Three experiments, presented in chapters 4,5,and 6, use a tunable laser diode as a source of input Stokes photons. The first experiment, presented in chapter 4, shows that the input Stokes signal can effectively couple to a Raman amplifier. This experiment will show that only a few photons in the input Stokes are needed to dominate the quantum noise (spontaneous emission). The second experiment, presented in chapter 5, involves imaging the amplified Stokes beam at the exit of the Raman amplifier. The experimental results are not explained by previous work that only considered gain guiding but rather are in agreement with the predictions of gain and index guiding. Finally, the last experiment, to be considered in chapter 6, examines the Stokes output energy as a function of detuning. It is found that the peak Stokes output occurs when the input Stokes signal is tuned to the blue side of the Raman resonance in agreement with the predictions of the theory which includes both gain and index guiding.

Chapter 7 contains concluding remarks on how index guiding affects the growth of the amplified Stokes beam in a Raman amplifier. Possible future experiments are also mentioned.

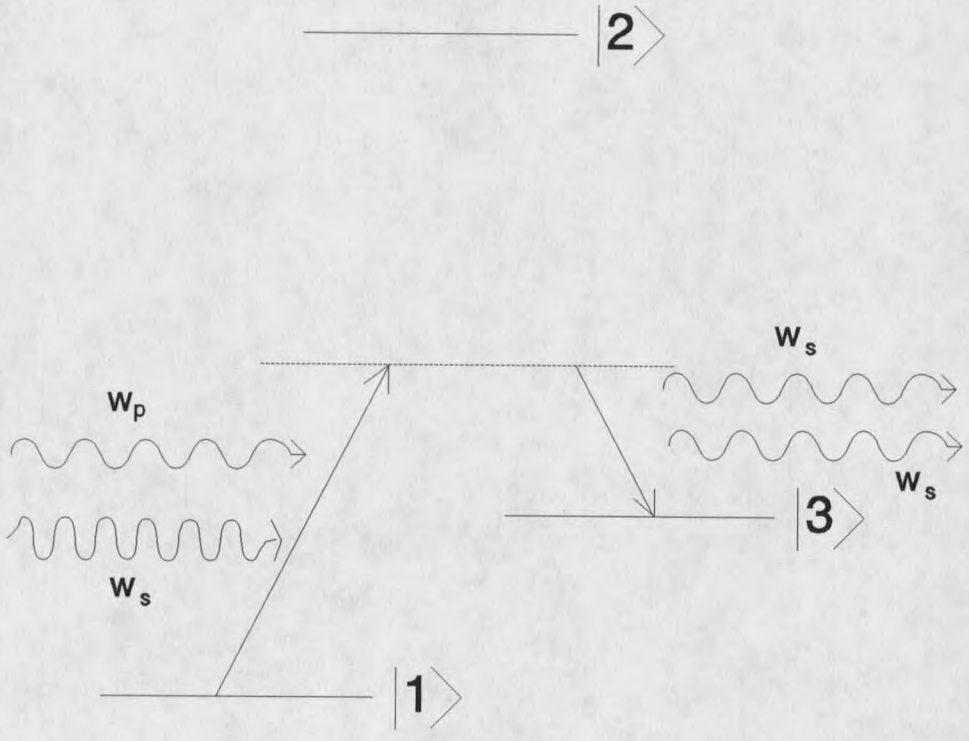


Figure 1 Schematic energy level diagram for Raman scattering

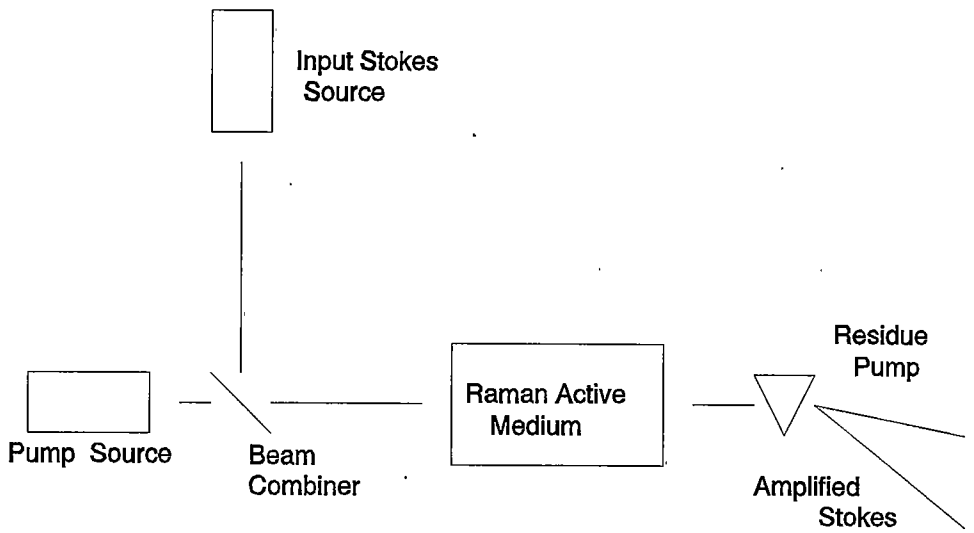


Figure 2 Simplified experimental setup to study stimulated Raman scattering

CHAPTER 2

THE WAVE EQUATION AND METHOD OF SOLUTION

Introduction

The mathematical formalism developed in this chapter allows us to numerically look at solutions to the wave equation that describes the Raman amplifier. First, the wave equation that describes the Raman amplifier is presented. The nonlinear Raman susceptibility is presented next. The nonlinear Raman susceptibility results from the H_2 molecule being driven by the beating of the Stokes and pump fields during the scattering process. Next, some limiting case solutions to the wave equation are studied. These solutions aid in understanding how the real and imaginary parts of the nonlinear Raman susceptibility affect the amplified Stokes field. Finally, two different methods of solution to the wave equation are presented which depend on modal expansions of the Stokes field. As mentioned in the first chapter, expanding the Stokes field over a Gauss-Laguerre basis allows one to describe a gaussian input in terms of a single mode. Also, more complicated inputs to the Raman amplifier are more easily described in terms of the

orthogonal Gauss-Laguerre basis than the nonorthogonal modal basis. While the Gauss-Laguerre basis is useful for describing the input into the Raman amplifier, the nonorthogonal modal basis is useful for describing the Raman amplifier output because only one nonothogonal mode is needed to describe the amplifier output in the high gain limit. Since the choice of basis is not obvious, the solution to the wave equation using both a Gauss-Laguerre basis and a nonorthogonal basis is presented later in this chapter.

Wave Equation

In the work done in this thesis, we are interested in describing the Raman amplifier in the steady state paraxial limit. The three dimensional wave equation that describes the Raman amplifier is written

$$\nabla_T^2 E_s(z,r_T) - 2ik_s \frac{\partial}{\partial z} E_s(z,r_T) = -\frac{4\pi\omega_s^2}{c^2} \chi_{NL} \left|E_p\right|^2 E_s(z,r_T) \qquad 2.1$$

where $\nabla_T^2 = \frac{\partial^2}{\partial x^2} + \frac{\partial^2}{\partial y^2}$ is the transverse laplacian, $E_s(z,r_T)$ is the slowly varying Stokes field, k_s is the Stokes wavevector, ω_s is the frequency of the Stokes field, c is the speed of light, χ_{NL} is the nonlinear Raman susceptibility and E_p is the pump field. The wave equation is derived in appendix A. The fully transient equations that describe the Raman amplifier are presented in appendix B along with a link to the above wave equation in the steady state limit.

The Nonlinear Raman Susceptibility

The nonlinear Raman susceptibility, χ_{NL}, is responsible for the Raman gain, gain guiding effects, and index guiding effects. The nonlinear Raman susceptibility in vibrational Raman scattering from diatomic hydrogen results from an induced dipole moment of the H_2 molecule due to the beating of the pump and Stokes field[1]. In this case we can let the vibrational frequency, ω_v, of the H_2 molecule define the Raman resonance. In appendix C the H_2 molecule is modeled as a damped driven harmonic oscillator with a resonant frequency ω_v. This model yields a nonlinear Raman susceptibility that can be written

$$\chi_{NL} = \frac{N\left(\left.\frac{\partial\alpha}{\partial X}\right|_0\right)^2}{16m\omega_v}\left(\frac{\Delta}{\Delta^2+\frac{\gamma^2}{4}} + i\frac{\frac{\gamma}{2}}{\Delta^2+\frac{\gamma^2}{4}}\right) \qquad 2.2$$

where N is the number density of H_2 molecules, α is the molecular polarization, m is the reduced mass of the H_2 molecule, $\Delta = \omega_v - (\omega_p - \omega_s)$ is the detuning away from the Raman resonance, and γ is related to the collisional dephasing rate, Γ, by the relationship $\Gamma = \gamma / 2$.

A definition is made for the Raman susceptibility χ_R such that

$$\chi_R = \chi_{NL}\left|E_p\right|^2 \qquad 2.3$$

One can write the Raman susceptibility from Eq.2.2 and Eq.2.3 as

$$\chi_R = \frac{N\left(\frac{\partial\alpha}{\partial X}\Big|_0\right)^2}{16m\omega_v}\left(\frac{\Delta\left|E_p\right|^2}{\Delta^2+\frac{\gamma^2}{4}} + i\frac{\frac{\gamma}{2}\left|E_p\right|^2}{\Delta^2+\frac{\gamma^2}{4}}\right) \qquad 2.4$$

Approximate Solutions To The Wave Equation

Before the solution to the wave equation, Eq.2.1, is presented in its full detail, some approximations are made to simplify the wave equation. Two objectives are reached in studying the simplified wave equation. The first objective is to cast the Raman susceptibility in terms of the parameters that are used in the literature such as k_s, the Stokes wavevector, $g(z,r_T)$, the gain profile, Δ, the detuning, and Γ, the collisional dephasing rate. The second is to obtain an understanding of how the Raman susceptibility influences the Stokes field.

The Raman susceptibility for a molecule can be written as $\chi_R = \chi' - i\chi''$ where the real and imaginary parts of the Raman susceptibility are defined in Eq.2.4. The constants in Eq.2.4 are determined by requiring that the Stokes growth predicted by the wave equation (Eq.2.1) be equal to the Stokes growth given in Refs.[29,30]. The results in Refs.[29,30] were derived under the assumption that no index guiding occurred

($\chi' = 0$) and diffraction of the Stokes field was negligible ($\nabla_T^2 E_s(z, r_T) \approx 0$). With these approximations the wave equation (Eq.2.1) can be written

$$\frac{\partial E_s(z)}{\partial z} = -\frac{2\pi\omega_s^2}{k_s c^2}\chi'' E_s(z) \qquad 2.5$$

which has

$$E_s(z) = E_s(0)e^{-\frac{2\pi\omega_s^2}{k_s c^2}\chi'' z} \qquad 2.6$$

as the solution for the field. Squaring the field leads to the Stokes intensity and the Stokes intensity is written

$$I_s(z) = I_s(0)e^{-\frac{4\pi\omega_s^2}{k_s c^2}\chi'' z} \qquad 2.7$$

On the other hand, Refs.[29,30] show that the Stokes intensity is

$$I_s(z) \propto e^{gz\frac{\Gamma^2}{\Delta^2+\Gamma^2}} \qquad 2.8$$

comparing Eqs.2.7 and 2.8 we obtain $-\frac{4\pi\omega_s^2}{k_s c^2}\chi'' = g\frac{\Gamma^2}{\Delta^2+\Gamma^2}$. Combining this result with Eq.2.4 allows us to write the Raman susceptibility as

$$\chi_R = \frac{k_s c^2}{4\pi\omega_s^2} g(z,r_T)\left(\frac{\Delta\Gamma}{\Delta^2+\Gamma^2} + i\frac{\Gamma^2}{\Delta^2+\Gamma^2}\right) \qquad 2.9$$

where the gain $g \to g(z,r_T)$ has been included to allow for the spatial variation of the gain profile.

Some insight into the effects of χ' and χ'' can be gleaned by solving the wave equation under the assumption that the diffraction of the Stokes field is negligible, $(\nabla_T^2 E_s(z,r_T) \approx 0)$. The wave equation is written

$$\frac{\partial E_s(z,r_T)}{\partial z} = \frac{2\pi\omega_s^2}{ik_s c^2}(\chi' - i\chi'')E_s(z,r_T) \qquad 2.10$$

The solution to Eq.2.10 is a simple exponential

$$E_s(z,r_T) = E_s(0,r_T)e^{-\frac{2\pi\omega_s^2}{k_s c^2}\chi''z - i\frac{2\pi\omega_s^2}{k_s c^2}\chi'z} \qquad 2.11$$

where $E_s(0,r_T)$ is the input Stokes field. From Eq.2.11, the imaginary part of the Raman susceptibility, χ'', leads to gain (absorption) if $\chi'' < 0$ ($\chi'' > 0$). Also from Eq.2.11 the real part of the Raman susceptibility, χ', leads to a phase shift. The transverse variation in the real part of the Raman susceptibility which results from the gain profile results in a phase shift that varies in the transverse direction. This phase shift can be thought of as caused by an index of refraction and is analogous to a phase shift resulting from a field passing through a lens. The real part of the Raman susceptibility can be thought of as creating an effective lens that can focus or defocus the Stokes beam and this leads to index guiding.

Solution To The Wave Equation

The wave equation is solved using a modal expansion of the Stokes field. The question of which basis to use for the expansion of the Stokes field is a difficult one. Ideally, the Stokes field would be described throughout the Raman amplifier by a single mode of the basis chosen. A Gauss-Laguerre basis[24,27] allows the input to be written as a single mode. The susceptibility couples this single input mode to several higher order modes with the same cylindrical symmetry as the gain but with different radial profiles. Coupling a single input mode to several modes at the exit of the Raman amplifier allows for the changes in the spatial structure of the amplified Stokes. A second more complicated basis that can be used to describe the Stokes field in a Raman amplifier is the nonorthogonal modal basis[17-22]. This basis has the nice property that only the lowest

order nonorthogonal mode is needed to describe the output of the Raman amplifier[19]. However, the gaussian input signal must be expanded over the more complicated nonorthogonal basis. Solutions to the wave equation using both a Gauss-Laguerre and nonorthogonal basis are presented in this section.

The Gauss-Laguerre Basis

Using the wave equation (Eq.2.1) and the Raman susceptibility (Eq.2.4), the Raman amplifier is described by

$$\nabla_T^2 E_s(z,r_T) - 2ik_s \frac{\partial E_s(z,r_T)}{\partial z} + ik_s g(z,r_T)\left(\frac{\Gamma^2}{\Delta^2+\Gamma^2} - i\frac{\Gamma\Delta}{\Delta^2+\Gamma^2}\right)E_s(z,r_T) = 0 \qquad 2.12$$

The wave equation includes the real and imaginary parts of the Raman susceptibility with Δ, the detuning from the Raman resonance and Γ, the Raman linewidth[31], explicitly included in the wave equation. The assumption that the spontaneous emission is negligible has been used and therefore no terms are needed in Eq.2.12 to account for the spontaneous emission. The validation of this assumption will be discussed more in chapter 4.

The focused nature of the pump beam is taken into account in the gain profile. In this work we will consider a focused gaussian gain profile [19,24,27,32]

$$g(z,r)=\frac{4G}{k_g\omega_g^2(z)}e^{-2r^2/\omega_g^2(z)} \qquad 2.13$$

where G is related to the plane wave gain coefficient[33], k_g is the pump laser wavevector, the gaussian beam waist is $\omega_g(z)=\omega_g(0)\sqrt{1+(z/z_0)^2}$, r is the magnitude of the transverse radius vector r_T, and z_0 is the Rayleigh range of the focused gaussian profile. The gain profile has rotational symmetry about the z axis and, therefore, it will be convenient to work in cylindrical coordinates.

The wave equation is similar to a wave equation solved by Perry et.al.[27] and the details of their solution are presented in Ref.[27]. A brief outline is presented here with the changes needed to account for χ' and the consequent index guiding effects. The Stokes field is expanded over a complete set of orthonormal Gauss-Laguerre modes $U_p^l(z,r_T)$. The Gauss-Laguerre modes are the solution to Eq.2.1 when the Raman susceptibility is set equal to zero. These modes solve the wave equation for free space propagation and are referred to as the modes of free space. The Gauss-Laguerre modes are defined in appendix D along with plots of some lower order modes.

The Stokes field is written as an expansion of the Gauss-Laguerre modes as

$$E_s(z,r_T)=\sum_{p,l}V_p^l(z)U_p^l(z,r_T) \qquad 2.14$$

where $V_p^l(z)$ are the field expansion coefficients. Substituting Eq.2.14 into Eq.2.12 and using the orthonormal properties of the Gauss-Laguerre modes yields the following set of linear coupled differential equations in z for the field expansion coefficients

$$\frac{dV_{p'}^{l'}}{dz} = \sum_{p,l} G_{p',p}^{l',l}(z) V_p^l(z) \qquad 2.15$$

where

$$G_{p',p}^{l',l} = \frac{1}{2}\left(\frac{\Gamma^2}{\Delta^2+\Gamma^2} - i\frac{\Gamma\Delta}{\Delta^2+\Gamma^2}\right)\int_0^{2\pi} d\varphi \int_0^{\infty} r dr\left[U_{p'}^{l'*}(z.r_T)\, g(z,r_T)\, U_p^l(z,r_T)\right] \qquad 2.16$$

Substituting the focused gaussian gain profile from Eq.2.13 and noting that the integration over φ results in non zero terms only when $l = l'$, the following expression for $G_{p',p}^{l}$ is obtained

$$G_{p',p}^{l} = G\frac{2\mu}{\omega_g^2(z)k_g}\left(\frac{\Gamma^2}{\Delta^2+\Gamma^2} - i\frac{\Gamma\Delta}{\Delta^2+\Gamma^2}\right) e^{-2i(p'-p)\tan^{-1}(z/z_0)} Q_{p',p}^{l}(\mu) \qquad 2.17$$

where the parameter $\mu = \lambda_p / (\lambda_p + \lambda_s)$ is defined as the mode filling factor with $\lambda_p(\lambda_s)$ the pump (Stokes) wavelength and $Q_{p',p}^{l}(\mu)$ is a polynomial in powers of μ and

is defined in appendix E. The fact that only nonzero terms result from $l = l'$ can be argued on the physical grounds that the modes which describe the Stokes field must have the same angular dependence as the gain.

The important substitution of variable

$$\theta = \tan^{-1}(z / z_0) \tag{2.18}$$

is made to fold out the focusing nature of the problem. The equation for the field expansion coefficients becomes

$$\frac{dV^l_{p'}(\theta)}{d\theta} = \sum_p M^l_{p',p}(\theta) V^l_p(\theta) \tag{2.19}$$

where

$$M^l_{p',p}(\theta) = \mu G \left(\frac{\Gamma^2}{\Delta^2 + \Gamma^2} - i \frac{\Gamma\Delta}{\Delta^2 + \Gamma^2} \right) Q^l_{p',p}(\mu) e^{-2i(p'-p)\theta} \tag{2.20}$$

The solution for the field expansion coefficients is

$$V^l_{p'}(\theta) = \sum_p A^l_{p',p}(\mu, G; \theta, \theta_m) V^l_p(\theta_{in}) \tag{2.21}$$

where the matrix elements $A^{l}_{p',p}(\mu, G; \theta, \theta_{in})$ are defined in appendix E, θ_{in} defines the input of the Raman amplifier, and θ defines the location in the Raman amplifier. The field expansion coefficients, $V^{l}_{p}(\theta_{in})$, are used to represent the input Stokes signal. When the Raman amplifier is seeded with a gaussian input signal, only the p=l=0 element of $V^{l}_{p}(\theta_{in})$ will be nonzero and the input Stokes power will be proportional to $\left|V^{0}_{0}(\theta_{in})\right|^{2}$. In this case the sum in Eq.2.21 will drop out.

Because only the p=l=0 element is needed to describe the input mode, the Gauss-Laguerre modes are a convenient choice for the Stokes field expansion. However, the coupling element $G^{l}_{p',p}$ couples this single input mode to several output modes for each individual l. The fact that many modes can couple together allows the amplified Stokes beam to have a different combination of spatial modes than the input Stokes signal and hence the amplified Stokes can have a significantly different spatial structure than the input Stokes signal. Notice however, that since the gain does not couple the input field to modes with different angular indices ("l" values), it is necessary to solve the above matrix equation for l=0 only.

The Nonorthogonal Basis

The wave equation presented in Eq.2.12 and the gain profile presented in Eq.2.13 are again the starting point. However, instead of expanding the Stokes field over the

Gauss-Laguerre basis, it is now expanded over a nonorthogonal basis[17-22]. The solution presented here is very similar to the solution presented in Ref.[19] and only a brief outline of the solution is presented here to show the changes needed to include the real part of the Raman susceptibility which allows for index guiding effects. The Stokes field is written as an expansion over the nonorthogonal modes as

$$E_s(z,r_T)=\sum_{n,l} a_n^l(z)\Phi_n^l(z,r_T) \qquad 2.22$$

where $a_n^l(z)$ is the amplitude of the nonorthogonal mode $\Phi_n^l(z,r_T)$. The nonorthogonal modes are required to satisfy the eigenvalue equation

$$\left(\nabla_T^2-2ik_s\frac{\partial}{\partial z}+ik_s g(z,r_T)\left(\frac{\Gamma^2}{\Delta^2+\Gamma^2}-i\frac{\Gamma\Delta}{\Delta^2+\Gamma^2}\right)\right)\Phi_n^l(z,r_T)=\lambda_n^l\frac{4ik_s}{k_g\omega_g^2(z)}\Phi_n^l(z,r_T) \qquad 2.23$$

The nonorthogonal modes are written as a summation over the free space Gauss-Laguerre modes. The summation in this case is only over the radial indices of the Gauss-Laguerre modes because the gain profile has rotational symmetry and only the l=0 angular indice has the proper rotational symmetry to match the gain profile. The nonorthogonal modes are written

$$\Phi_n^l(z,r_T)=\sum_p b_{n,p}^l U_p^l(z,r_T) \qquad 2.24$$

where $b_{n,p}^l$ are the free space mode coefficients. Making the change of variable $\theta=\tan^{-1}(z/z_0)$ and using Eq.2.23 and Eq.2.24, the equation of motion for the free space mode coefficients becomes

$$\frac{\partial b_{n,p'}^l}{\partial\theta}-\sum_p b_{n,p}^l e^{-2ip'\theta}K_{p',p}^l(\mu)e^{2ip\theta}=\lambda_n^l b_{n,p'}^l \qquad 2.25$$

where

$$K_{p',p}^l(\mu)=\frac{\mu G z_0}{\pi\omega_g^2(0)}\left(\frac{\Gamma^2}{\Delta^2+\Gamma^2}-i\frac{\Gamma\Delta}{\Delta^2+\Gamma^2}\right)Q_{p',p}^l(\mu) \qquad 2.26$$

where $Q_{p',p}^l(\mu)$ is defined in appendix E.

Equation 2.25 can be transformed into an operator equation by defining the vector b_n^l which represents the free space mode coefficients $\{b_{n,p}^l\}$ and writting $K_{p',p}^l$ as a matrix K^l. The operator equation becomes

$$\left[\frac{\partial}{\partial\theta}-e^{-iH\theta}K^l e^{iH\theta}-\lambda_n^l\right]b_n^l=0 \qquad 2.27$$

where $H^l_{p',p} = 2p\delta_{p',p}$. The solution to Eq.2.27 is

$$b^l_n = e^{-iH\theta}\lambda^l_n \qquad 2.28$$

where λ^l_n satisfy the eigenvalue equation

$$\left(K^l + iH\right)\chi^l_n = \lambda^l_n \chi^l_n \qquad 2.29$$

The details of the solution to Eq. 2.29 are presented in Ref[19]. Finally, the nonorthogonal mode can be written

$$\Phi^l_n(z, r_T) = \sum_p e^{-2ip\theta} U^l_p(z, r_T)\lambda^l_{n,p} \qquad 2.30$$

The Stokes field is written as a superposition of the nonorthogonal modes. The nonorthogonal modes have been calculated above. Next, the expansion coefficients (a^l_n) need to be calculated. Substituting the field expansion (Eq.2.22) into the wave equation leads to the equation

$$\sum_n -2ik_s\left(\frac{\partial a_n^l}{\partial z}+\lambda_n^l\frac{2}{k_g\omega_g^2(z)}\right)=0 \qquad 2.31$$

The solution to Eq.2.31 is

$$a_n^l(z)=a_n^l(0)e^{-\frac{2}{k_g\omega_g^2(z)}\lambda_n^l} \qquad 2.32$$

where $a_n^l(0)$ is the projection of the input Stokes signal on the Φ_n^l nonorthogonal mode. The amplified Stokes field is finally constructed from Eqs.2.22, 2.30, and 2.32.

Armed with the solution to the wave equation we are now ready to study the effects of index guiding in a Raman amplifier.

CHAPTER 3

MODE STRUCTURE OF THE AMPLIFIED STOKES FIELD

Introduction

The effects of gain and index guiding on the amplified Stokes beam in a Raman amplifier are numerically studied in this chapter. The wave equation presented in chapter two is solved using both the nonorthogonal modal expansion and the Gauss-Laguerre modal expansion. These two different methods of solution yield the same results, as expected.

The wave equation was solved in chapter two for the limiting case of no diffraction, and we saw how the imaginary part of the Raman susceptibility led to gain and the real part of the Raman susceptibility led to a phase shift that is associated with an index of refraction. In the next section, physical arguments are made to describe how the gain leads to gain guiding and how the index of refraction leads to index guiding. Next, the phasefronts of the amplified Stokes field are studied along with the spatial structure of

the amplified Stokes field. Finally, some comments about enhanced coupling into a Raman amplifier are presented in terms of the mode structure and detuning.

Physical Arguments For Gain And Index Guiding

Gain guiding works to narrow the amplified Stokes beam in the following way. For a focused gaussian pump beam, the center of the gain profile, which is proportional to the pump intensity, amplifies the center of the signal more than the wings because the gain is larger near the center of the gain profile. Because the center of the amplified Stokes grows more than the wings, the amplified Stokes beam narrows.

Figure 3 is a graphic representation of gain guiding. The dot-dashed line represents a gaussian gain profile with a maximum gain of 2.5. The dashed line is the input signal and has a maximum intensity of 1 and the full width at half maximum (FWHM) is shown. The amplified field is found by multiplying the input signal times the exponential of the gain (exponential growth). The amplified field is shown as the solid line in Fig.3 and the FWHM is labeled. Note that the FWHM of the amplified field is narrower than the FWHM of the input signal. The exponential growth used to generate the amplified field for Fig.3 is a good model for the amplification in a Raman amplifier.

A review of a focusing lens will help in the physical explanation of how index guiding works. Figure 4 shows a plane wave impinging on a lens from the left. The optical path length which is a product of the length which the light travels multiplied by the index of refraction of the material through which the light travels is larger at the

center of the lens than at the wings of the lens. The phasefront is retarded more near the center of the lens because the light travels through a larger optical path length than the wings.. This is why the phasefront appears curved after the lens. As the beam propagates further, diffraction causes the phasefront to change as shown in Fig.4.

The phase shift of the amplified Stokes field in a Raman amplifier is proportional to the real part of the Raman susceptibility as was seen in Eq.2.16. The real part of the Raman susceptibility is written $\chi' = g(z, r_T)\left(\frac{\Gamma\Delta}{\Delta^2 + \Gamma^2}\right)$. The gain profile is proportional to the pump laser intensity and is a gaussian. When the input Stokes is detuned to the blue side of the Raman resonance so that $\Delta \neq 0$, the real part of the Raman susceptibility causes the Stokes field to see an optical path length similar to that shown in Fig.4. Hence, when the Stokes seed is detuned to the blue side of the Raman resonance, the amplified field experiences an effective lens caused by the phase shift related to the real part of the Raman susceptibility. The ability of the Raman medium to focus the Stokes beam is referred to as index guiding.

Mode Structure Of The Amplified Stokes Field

The phasefronts and spatial structure of the lowest order nonorthogonal mode and gaussian input Stokes signal are studied in this section for two cases. The first case occurs when the input signal is tuned exactly to the Raman resonance, $\Delta = 0$, and therefore the Raman susceptibility is purely imaginary which leads to gain without any index guiding effects. This case will allow us to understand how gain guiding effects the

nonorthogonal mode. In the second case, $\Delta \neq 0$, and the Raman susceptibility contains both an imaginary and a real term. In this case the Raman susceptibility leads to an index of refraction which gives rise to index guiding. Thus, in the second case both index and gain guiding are considered.

Unless otherwise noted, the following parameters which describe the Raman amplifier are used in the calculations for this chapter. For parameters that are typical of Raman amplifier experiments, the difference in the phasefronts would be difficult to show in the figures. Therefore the waist and wavelengths were chosen so that the differences between the phasefronts can easily be seen in the figures. This makes the physical explanation of the mode structure and coupling easier to understand. The Rayleigh range was set at $\sqrt{2}$ cm for both the pump and input Stokes signal. A gain of G=3 and a pump beam waist of $\omega_g(0) = 1\,\text{cm}$ were used. The Raman linewidth was set at 3000MHz and the detuning used was $\Delta = 0\,\text{MHz}$ for the on resonance case and $\Delta = \pm 300\,\text{MHz}$ for the off resonance cases. The entrance to the Raman amplifier was at $z / z_{0g} = -2$.

Figure 5 shows the phasefronts for case 1 in which $\Delta = 0$. The solid line shows the phasefronts for the lowest order nonorthogonal mode while the dashed line shows the phasefronts for the gaussian input Stokes mode. The phasefronts are plotted at various locations in the cell defined by z/z_{0g} with the gaussian input signal mode focusing at $z/z_{0g}=0$. For $z/z_{0g}<0$ notice that the curvature of the phasefronts indicate that input signal is focusing while for $z/z_{0g}>0$, the curvature of the phasefronts indicates that the input

signal is diffracting. This is not surprising since the input Stokes signal is a focused gaussian. However, the phasefronts of the nonorthogonal mode are much more complicated and very different than the gaussian input Stokes signal. The phasefronts for case 1 result from competition between gain guiding and diffraction, as discussed below. Notice that the phasefronts of the nonorthogonal mode and gaussian input Stokes signal are poorly matched. This indicates that the Raman amplifier is not being used efficiently[30,35].

Gain guiding has the effect of narrowing the Stokes beam as it grows in the Raman amplifier. However, as the Stokes beam becomes narrower it wants to diffract faster. The competition between gain narrowing and diffraction cause the nonorthogonal mode to have phasefronts which are swept back from the input signal gaussian mode indicating a higher rate of diffraction for the nonorthogonal mode which is compensated by the gain narrowing.

Figure 6 shows the spatial structure of both the nonorthogonal mode (solid line) and the gaussian input signal mode (dashed line). The nonorthogonal mode is narrower than the gaussian mode because of gain guiding. It is interesting to note that this result holds throughout the Raman amplifier which may seem surprising because we would expect the narrower nonorthogonal mode to diffract faster than the gaussian mode. The nonorthogonal mode stays narrower because gain guiding can compensate for the diffraction.

Figure 7 shows the index effect when the input Stokes signal is detuned to the blue side of the Raman resonance. As before, the dashed line is the phasefront of the gaussian input Stokes signal and the solid line is the phasefront of the nonorthogonal mode when the detuning is set equal to zero. The dot-dashed line is the phasefront of the nonorthogonal mode when the input signal is detuned to the blue side of the Raman resonance. When the input Stokes signal is detuned to the blue side of the Raman resonance, the index guiding effect changes the phasefront much like a focusing lens. The phasefronts are swept back less when the input Stokes signal is tuned to the blue side of the Raman resonance than when $\Delta = 0$ indicating focusing is occurring. The fact that the index of refraction is trying to guide the Stokes beam gives rise to the term index guiding.

Figure 8 shows the index effect when the input Stokes signal is tuned to the red side of the Raman resonance. The dashed and solid lines are the same as in Fig.7. The dot-dashed line is the phasefront when the input Stokes signal is detuned to the red side of the Raman resonance. The phasefronts on the red side of the resonance are swept back more than when $\Delta = 0$ indicating defocusing is occurring.

The spatial structure of the nonorthogonal mode at $z/z_{0g}=0$ is shown in Fig.9. The dashed and solid lines are the same as in Fig.6 and are shown again for reference. The dot-dashed line shows the intensity profile of the amplified Stokes when the input Stokes signal is detuned to the blue side of the Raman resonance. The dotted line is the intensity profile when the input signal is detuned to the red side of the Raman resonance. When

the input Stokes signal is detuned to the blue (red) side of the Raman resonance the Stokes profile is narrower (wider) than when the input Stokes signal is tuned to the Raman resonance and these results are consistent with the phasefront picture. The use of index guiding to enhance the output of the Raman amplifier is discussed in the next section.

Enhanced Performance of a Raman Amplifier

Efficient coupling of an input signal into an optical amplifier requires that the input signal mode strongly overlap the dominant amplifier mode which has the highest growth rate[19,30,35]. When the structure of the input signal mode, including the phasefronts, exactly matches the dominant amplifier mode, all of the input signal is available to gain at the highest growth rate. However, if the pump wavelength is different than the signal wavelength or nonlinear effects are occurring such as gain and index guiding in the optical amplifier, it may not be clear how, or even if, the input signal mode can exactly overlap the dominant amplifier mode. If, for example, the phasefronts of the input signal mode and dominant amplifier mode are not matched, interference effects can lower the coupling between these two modes thus diminishing the amplifier performance. Manipulating the structure of the input signal mode to match the amplifier mode can increase the output of the amplifier by forcing the input signal to overlap the dominant amplifier mode.

The overlap of the phasefronts of the gaussian input signal mode and lowest order nonorthogonal mode is poor as seen in Figs.5,7,and 8 when the input mode and lowest order nonorthogonal mode focus at the same location with the same Rayleigh range. By changing the position of focus and Rayleigh range of the input Stokes signal, we can force the phasefronts to better overlap the lowest order nonorthogonal mode and hence enhance the input coupling of the Raman amplifier.

Figure 10 shows that by changing the location of focus and Rayleigh range of the input signal mode, its phasefronts can better overlap the lowest order nonorthogonal mode. The solid lines are the nonorthogonal modes phasefronts whose shape is determined by the Rayleigh range and power of the pump laser. We consider these phasefronts to be fixed and show that by varying the characteristics of the input Stokes signal can enhance coupling into the amplifier. The dashed lines are the phasefronts of the input signal mode with a Rayleigh range and location of focus the same as the pump. The dotted lines are the phasefronts for an input signal mode with a Rayleigh range of one half that of the pump and the focus shifted towards the front of the Raman amplifier. Notice that the dotted lines and solid lines match much better than the solid lines and dashed lines. This indicates that the input signal mode with the shorter Rayleigh range and shifted focus will better overlap the lowest order nonorthogonal mode and thus improve the performance of the Raman amplifier.

Figure 11 summerizes a more detailed study of how the shift in location of the focus can affect the output of the Raman amplifier. The dashed line shows the output of

the Raman amplifier as a function of the focal position of the input Stokes signal when the pump and input signal have the same Rayleigh range. The output Stokes energy has been normalized so that when the pump and input Stokes signal have the same Rayleigh range the output Stokes energy is unity. When $z_{0s}=z_{0g}$ the output of the Stokes signal is enhanced 5% by shifting the focus of the input signal towards the front of the Raman amplifier by approximately one half a Rayleigh range. The solid line is the output Stokes energy as a function of the relative focus when the Rayleigh range of the input signal is one half that of the pump. When the focus of the input Stokes signal is shifted towards the entrance of the Raman amplifier by approximately one Rayleigh range the output Stokes is increased by over 20%. The output Stokes is further increased when the input Stokes signal is tuned to the blue side of the Raman resonance. The dot-dashed line is the same as the solid line except that the input Stokes has been detuned to the blue side of the Raman resonance. The output is enhanced by over 40% when the input signal has been modified and tuned to the blue side of the Raman resonance. This implies that by carefully setting up an optical amplifier, the output can be significantly increased without changing the pump power.

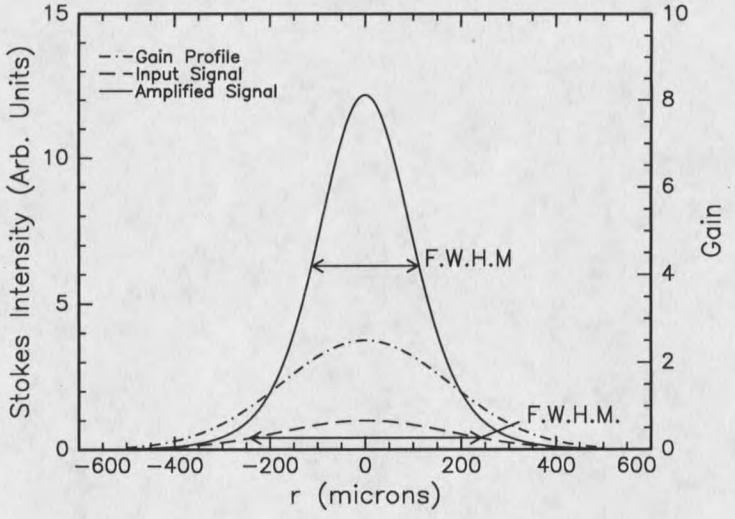


Figure 3 Plot to show how gain guiding works. The dot-dashed line represents the gaussian gain profile, the dashed line represents the transverse profile of the input beam and the solid line represents the transverse profile of the amplified beam.

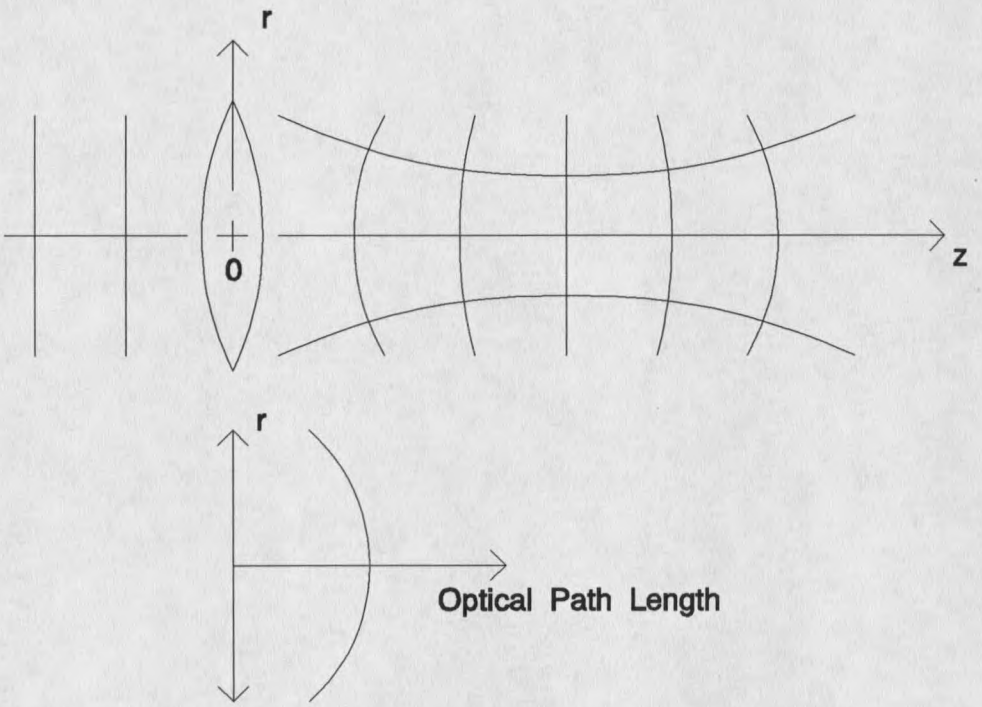


Figure 4 Plot to show the how a lens affects the phasefronts of an optical field. The bottom plot shows the difference in the optical path length for light traveling from z=-t/2 to z=t/2 where t is the thickness of the lens at r=0.

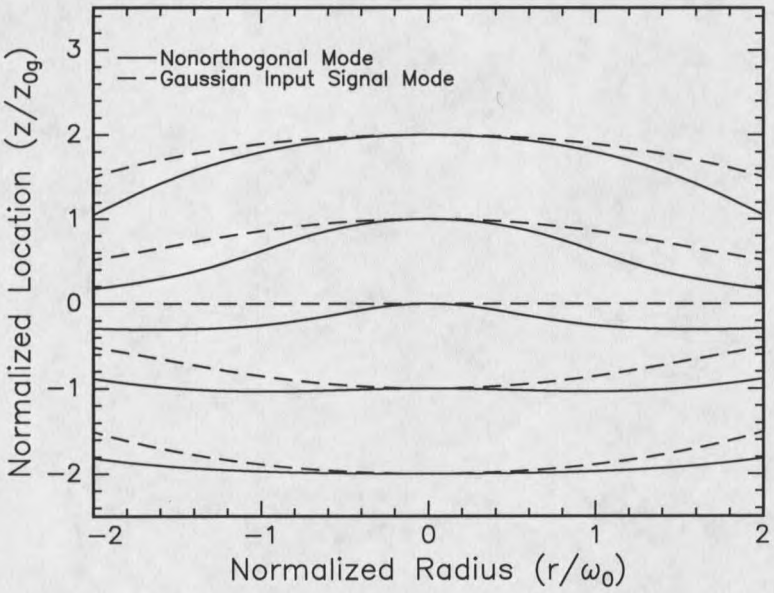


Figure 5 Plot of the phasefronts of the dominant nonorthogonal mode (solid line) and gaussian input signal mode (dashed line) at various locations in the Raman amplifier. The nonorthogonal modes are swept back from the gaussian input signal mode as a result of gain guiding and diffraction. The phase overlap of the two modes is poor indicating poor amplifier performance.

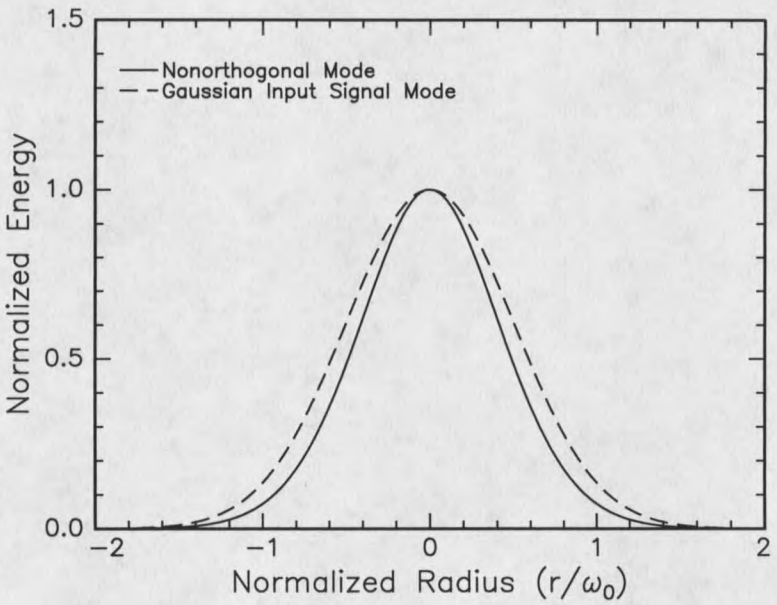


Figure 6 Plot of the spatial structure of the dominant lowest order nonorthogonal mode (solid line) and the gaussian input signal mode. The nonorthogonal mode is narrower throughout the Raman amplifier due to gain guiding.

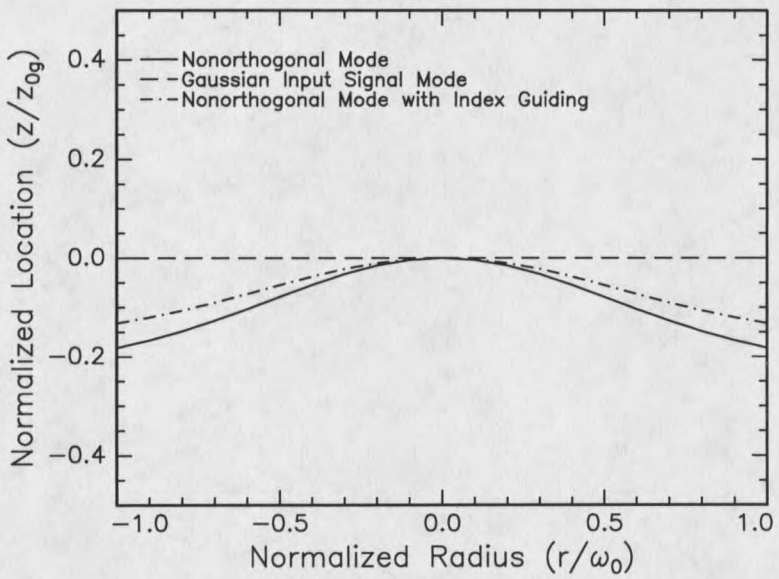


Figure 7 Plot of the phasefront of the dominant nonorthogonal mode including index guiding. The nonorthogonal mode for the on resonance case is shown as the solid line while the gaussian input signal mode is shown as a dashed line. The nonorthogonal mode including the effects of index guiding is shown as a dot-dashed line. The index effect when the input signal is tuned to the blue side of the Raman resonance acts as a lens which tries to focus the nonorthogonal mode and leads to less curvature of the phasefronts in this case.

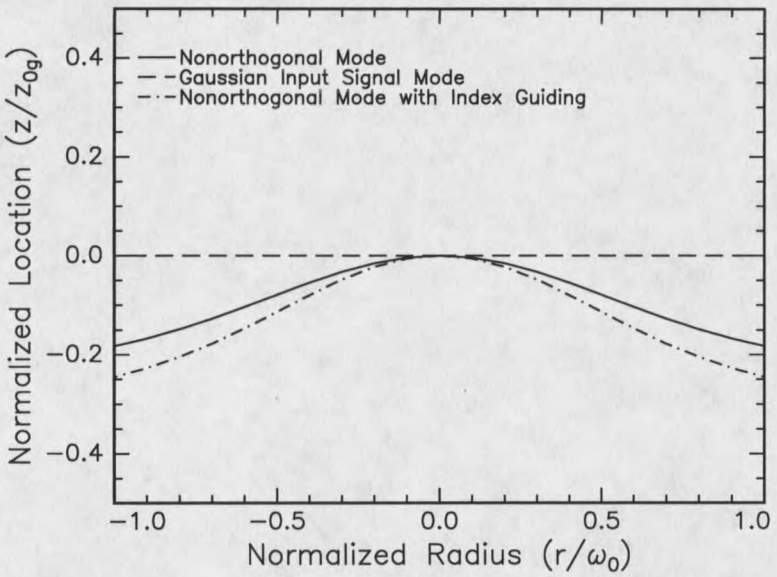


Figure 8 Same as figure 7 except with the input signal tuned to the red side of the Raman resonance. The index effect acts as a defocusing lens in this case.

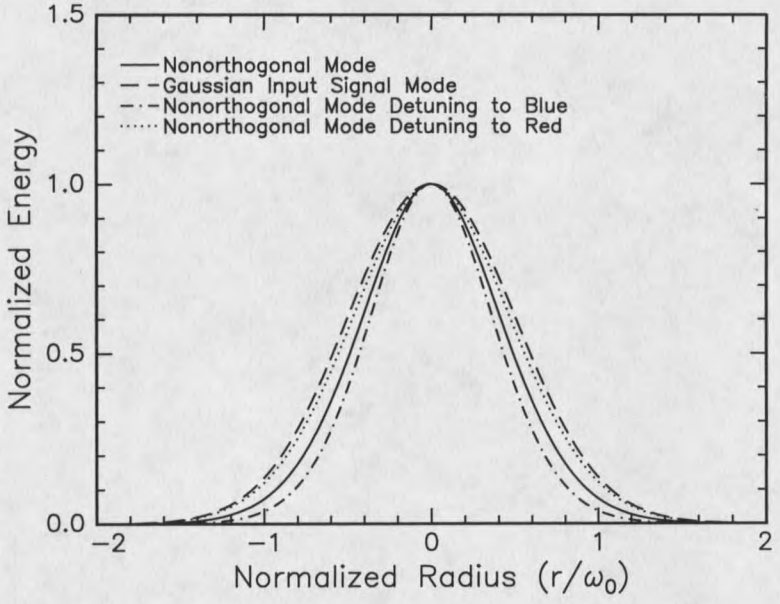


Figure 9 Plot of the spatial structure of the dominant nonorthogonal mode. The solid and dashed lines are the same as in figure 6 and are shown again for reference. The dot-dashed line shows the spatial structure of the nonorthogonal mode when the input is tuned to the blue side of the Raman resonance and the dotted line shows the spatial structure when the input signal is tuned to the red side of the Raman resonance. Tuning to the blue (red) side of the Raman resonance causes the nonorthogonal mode to become narrower (wider) than when the input signal is tuned on resonance.

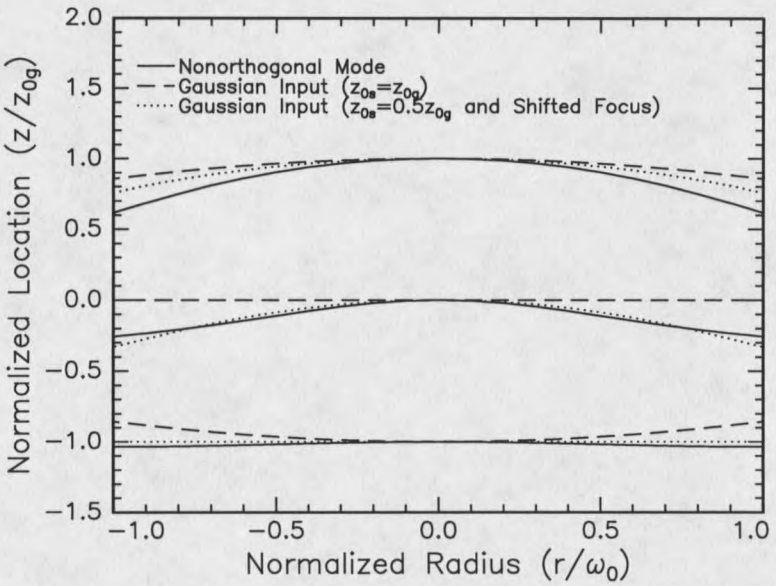


Figure 10 Plot of the phasefronts of the nonorthogonal mode (solid line), gaussian input signal mode (dashed line) and modified gaussian input signal mode (dotted line). The nonorthogonal mode and modified input signal match better than the nonorthogonal mode and unmodified input signal indicating the modified input signal enhances the performance.

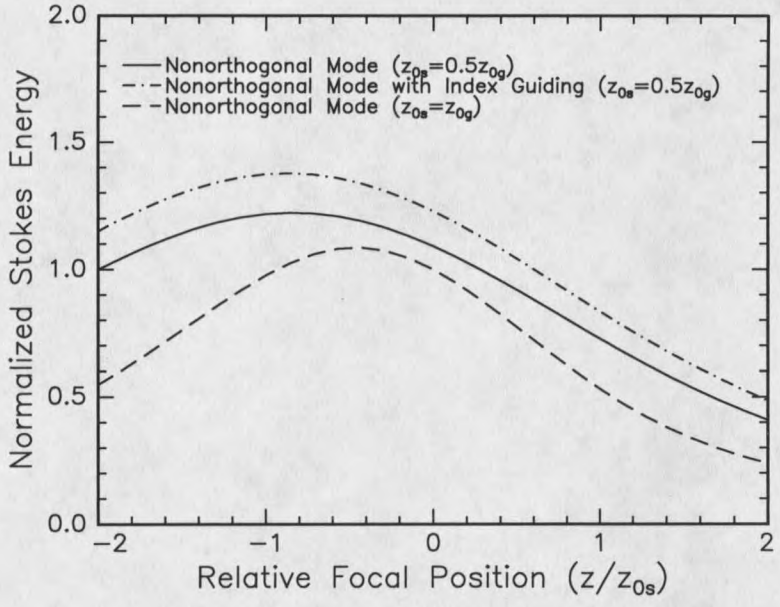


Figure 11 Plot of the normalized output Stokes energy as a function of relative focal position of the gaussian input signal and pump focus. When $z_{0s}/z_{0g}=1$, shifting the focus by approximately one half a Rayleigh range yields a 5% increase in the output Stokes energy. For $z_{0s}/z_{0g}=0.5$, shifting the focus of the input signal by approximately one Rayleigh range increases the Stokes output by 20%. When the input is detuned to the blue side of the Raman resonance, the Stokes output is increased by over 40%.

CHAPTER 4

SEEDING OF A RAMAN AMPLIFIER WITH A VISIBLE LASER DIODE

Introduction

Recent experiments have demonstrated that only a few photons of input into a Raman amplifier were enough to ensure that the amplified signal was larger than the amplified quantum noise[36,37]. However, in both of these experiments, as well as in most other Raman experiments that use an input Stokes signal, the seed input was obtained from a Raman generator. Since a Raman generator is initiated by spontaneous emission, the energy[38], frequency spectrum[39], and spatial characteristics[40] of the seed fluctuate by large amounts. These fluctuations can be avoided by using a tunable laser diode as the source for the input Stokes photons for the Raman amplifier.

Uchida et. al.[41] used an infrared laser diode to seed the 16 μm stimulated rotational Raman scattering in a multipass cell (MPC) with H_2 as the Raman active medium. When the input Stokes signal was input into the Raman amplifier, a significant enhancement of the Stokes conversion, as well as a large reduction in the pump threshold

was obtained. Nonetheless, their results were surprising, as the measured coupling efficiency of 0.1-0.2% was much lower than the theoretical prediction of 100%. They attributed the poor coupling to diffraction losses inherent in the MPC structure.

In this chapter, data is presented from an experiment that uses a tunable laser diode as an input Stokes signal for vibrational Raman scattering in H_2 in a MPC cell at visible wavelengths[30]. In this experiment we also find the enhancement in the Stokes conversion and the reduction of the pump threshold. However, we measured a coupling efficiency of 65% which approaches the theoretical maximum.

The seeding experiment discussed in this chapter is an experimental technique that will be used in the next two chapters to discuss the effects of index and gain guiding. This experiment is included in the thesis to show in detail how the seeding of a Raman amplifier works, to lend credence to the assumption made in the theory section that indeed an input Stokes signal can dominate the quantum noise and hence the spontaneous emission is negligible, and finally, to introduce key experimental apparatus that is needed for the experiments that study the effects of gain and index guiding.

Experiment

The experimental apparatus for the injection seeding experiment using a tunable laser diode as the source for the input Stokes signal is shown in Fig.12. The frequency-doubled output at 532nm of a pulsed, single mode, injection locked Nd:YAG laser was used to pump the Raman amplifier. The temporal profile of the pump laser was near

gaussian with a half width at half maximum (HWHM) of 3.5ns. The pump beam was mode matched into the MPC by use of a two lens system.

A beam splitter (B1 in Fig.12) placed before the MPC was used to direct part of the pump beam onto a Pulnix TM-745 charge coupled device (CCD) camera which monitored the pointing fluctuations of the pump beam. The pixel cell size of the CCD camera, which sets the resolution of the pointing fluctuation measurements, was 11 μm x 13 μm.

A New Focus continuous wave tunable laser diode with a center wavelength of 683nm and an output power of approximately 3mW was used as the source for the input Stokes signal for this experiment. In addition to a mechanical tuning range of ± 5nm, the laser diode has an electronic tuning range of 0.015nm over an externally applied voltage ramp of -3 to +3 volts. The laser diode was isolated from the rest of the experiment by a Faraday isolator. The Faraday isolator prevented unwanted feedback from affecting the performance of the tunable laser diode. The power of the input Stokes signal was measured with a power meter located behind a calibrated beamsplitter (B3 in Fig.12). A beamsplitter (B4) directed part of the seed beam into a temperature controlled high finesse cavity[42,43] (HFI). The details of the HFI's used in this and the following experiments are presented in the next section. The HFI used for this experiment[42] had a free spectral range of 4.98GHz and a measured finesse of 30,000 and was used to monitor the relative frequency of the input Stokes signal. The remainder of the input Stokes signal was coupled into a single mode optical fiber which allows a convenient way to

spatially filter the input Stokes signal. The input Stokes signal was then mode matched into the MPC by the use of a two lens system. A dichroic beamsplitter (B2 in Fig.12) was used to combine the 683nm input Stokes signal and the 532nm pump beam.

The MPC design was the same as that use in previous experiments[29] with the following changes: The mirror spacing was 1.98m, the mode matching confocal parameter was $b=2z_0=45.6$cm, and the number of passes was 11. The Raman amplifier for this experiment consisted of a cell filled with H_2 to a pressure of 34atm. The transmission after 11 passes was measured at 76% at the pump wavelength and 70% at the Stokes wavelength. After leaving the MPC, the pump and Stokes beams were separated by a Pelin-Broca prism. The output energy of the pump beam was measured with a pyroelectric energy detector. This permitted the cell transmission to be monitored for each shot. The Stokes output was measured with a silicon energy detector. In front of the Stokes detector was a narrowband filter centered at the Stokes wavelength to prevent any scattered pump radiation from entering the detector.

High Finesse Interferometers

HFI's[42,43] can be used to resolve narrow linewidths while large free spectral ranges are maintained. However, the ultimate usefulness of these HFI's depends on their frequency stability. Principle sources of long term instabilities or drifts for HFI's are spurious changes in mirror separation distance and fluctuations in the index of refraction

of the medium between the mirrors. The principle source of short term or shot to shot instability is the electronics used to drive the piezo which scans the mirrors.

Stability of the relative frequency measurement requires that the free spectral range (FSR), given by

$$FSR = \frac{c}{2nd} \qquad 4.1$$

where c is the speed of light, n is the index of refraction, and d is the mirror spacing, remains constant. Equation 4.1 shows that the free spectral range depends on the mirror spacing d and the index of refraction n. As thermal fluctuations cause interferometer components to expand or contract, the mirror spacing d will change. The index of refraction of the air between the mirrors is affected by variations in pressure and temperature, and this is discussed in Refs.44,45. As a numerical example, an isobaric change in temperature of 0.1°C results in an apparent frequency shift of 50MHz when 633nm light is used. On the other hand, an isothermal increase in pressure of 0.01atm results in an apparent frequency shift of 1400MHz. Since the pressure and temperature of the ambient laboratory air typically fluctuate by more than these amounts, it is imperative that the HFI be enclosed in a sealed, temperature controlled vessel.

The mirrors are the most important part of the interferometer. The finesse $\Im_R$ of the interferometer is related to the reflectivity of the mirrors by the relationship

$$\Im_R = \frac{\pi\sqrt{R}}{1-R} \qquad 4.2$$

where R is the reflectivity of the mirrors. Mirror reflectivities of better than 99.997% are available which corresponds to $\Im_R$>100,000. The mirrors used in the interferometer built for the experiments described in this and the next two chapters has a reflectivity of R>99.995%.

The curvature of the mirrors is important because it allows us to use a much smaller spot size than conventional flat plate Fabry Perot (FPFP) interferometers. The smaller spot size is due to the refocusing of the beam on each pass. The smaller spot size significantly reduces the problem of surface aberrations which limit the finesse of conventional FPFP interferometers to about 100. The mirrors used in this HFI have a radius of curvature of 1m.

Figure 13 shows a schematic of the HFI that was built to address the temperature and pressure issues presented in Refs.44,45. The mirrors have a 1m radius of curvature and a manufacturer quoted reflectivity of 99.995% at 633nm. A 2.54cm outside diameter by 2.54cm long piezoelectric transducer (PZT) is used to scan the mirrors. This is the smaller PZT used in the fig.13. The larger diameter PZT is used for temperature compensation as discussed below. The spacer flange is made of electrically insulating plexiglass. Three small screws placed 120° apart are used to connect the spacer flange to the spacer. The o-rings shown at the head of the screw allow for movement of the mirror without undue stress when the PZT expands. The PZT tubes are seated in recessed

groves in the spacer flange and are separated by an aluminum spacer. The scanning mirror is held in place at the front of the spacer by the inner PZT. The Corning ultra low expansion (ULE) tube contacts the PZT tube on the right hand side and sits in a recessed groove on the flange on the left. The depth of the recessed groove is chosen so the end of the ULE tube and the left hand mirror surface are in the same plane. This is important because we want only the ULE tube spacing the mirrors. The spacer flange and flange are held together by three nuts and bolts. The o-rings allow for motion of the spacer flange with respect to the flange caused by scanning the smaller diameter piezotube. The inner tube is made of aluminum and has an interference fit with the o-rings on the outside of the spacer flange and flange. The o-rings provide a first layer of vibration isolation. On the outside of the inner tube is a layer of sorbathane which provides a second layer of vibration isolation. The vacuum tube has an interference fit over the sorbathane.

The HFI was designed to attack the problem of thermal drift in the following way. The small diameter and large diameter PZT tubes are made of the same material. Any expansion in one tube should be canceled by the same expansion in the other tube. The only other relevant component left to consider in the thermal expansion is the ULE tube. The ULE tube was chosen as the spacer material because of its extremely low coefficient of thermal expansion α_E, which for ULE is less than 10^{-9} $(^{\circ}C)^{-1}$. The HFI is evacuated when in operation which alleviates any problems that arise due to pressure variations

The HFI is a nonconfocal cavity which is constructed of two spherical mirrors of radius R_m separated by a distance d, with $d<<R_m$. In general, the electric field inside the

cavity is expressed as an infinite set of spatial modes. However, the HFI is most useful when only one of these modes, usually the lowest order or fundamental mode is excited. Care must be taken when setting up the HFI so that these higher order spatial modes can be suppressed. The higher order spatial modes will be suppressed when the cavity is mode matched[42]. Mode matching is discussed in detail in Appendix F.

The high finesse interferometer discussed above and used in the experiments discussed in this thesis has the following performance parameters. The measured finesse was greater than 30,000 and the measured stability was better than 7MHz/Hr. The measured stability of the HFI is discussed in Ref.43.

Results

The results for the experiment with a nominal pump energy of 153 μJ are shown in Figs.14,15. The output Stokes energy is plotted versus the relative frequency of the input seed laser. Figure 14 is a plot of the raw data. The input pump energy was measured at 153 μJ with fluctuations as high as $\pm 15\ \mu J$ leading to large fluctuations in the output Stokes power as the steady state Stokes power grows as an exponential of the pump energy. It was also found that the pump beam at focus fluctuates by as much as $\pm 50\ \mu m$ in both the vertical and horizontal directions. In contrast, the input Stokes signal fluctuated by no more than $\pm 10\ \mu m$ in both the horizontal directions. As the e^{-2} intensity radius of the pump beam was 200 μm, pointing fluctuations also significantly affected the Stokes amplification. When only those shots centered within a 11 μm x

13 μm window and whose pump energy is $153 \pm 1\ \mu J$ are included, the effects of the beam pointing and pump energy fluctuations are surpressed. Approximately 2% of all shots collected met these requirements, and these are plotted in Fig.15.

The data in Fig.15 has been fitted to a gaussian using a least square fit. Using the collision dephasing rate of $\Gamma = 5.01 \times 10^9 GHz$[31], the plane wave gain coefficient of $2.5 \times 10^{-9} cm/W$[34] and a pump energy of 153 μJ, a gain narrowed lineshape with a HWHM of 128MHz is predicted[46]. The measure HWHM linewidth of 185MHz was predicted. The linewidth as a function of pressure of H_2 is studied more thoroughly in appendix G. Linewidth measurements as well as output Stokes energy measurements were also made at other pump energies ranging from 102 to 155 μJ. This range of pump energies was chosen so that the steady state Raman theory would be applicable. Linewidths measured at these other pump energies were found to be close to those measured at the pump energy of 153 μJ.

In Fig.16, the output Stokes energy for both seeded growth (+) and growth from spontaneous emission (Δ) have been plotted. The solid line is the predicted growth when an input Stokes signal was used while the dashed line is the predicted growth from spontaneous emission. A fully quantum mechanical theory was used for the spontaneous emission prediction[46]. The input Stokes signal was measured at 30nW. However to obtain a numerical estimate of the coupling efficiency we did a least squares fit of the data to a straight line for the seeded growth in Fig.16. The fit (not shown in Fig.16) yielded a slope of $(7.2 \pm 3.8) \times 10^4$. We obtain the coupling efficiency be forming the ratio

of the predicted seeded growth using a 30nW input Stokes signal with the least squares fit to the experimental data. This was found to be 65($\pm$45)%.

This experiment shows the key components needed for using a tunable laser diode to seed a Raman amplifier. This experiment also shows that large coupling efficiencies can be obtained and very small input Stokes signals can easily dominate the spontaneous emission. In fact, Fig.16 shows that with only a 30nW input Stokes signal the seeded growth is 2.5 orders of magnitude higher than the growth from spontaneous emission. For this reason we can neglect the spontaneous emission in the wave equation.

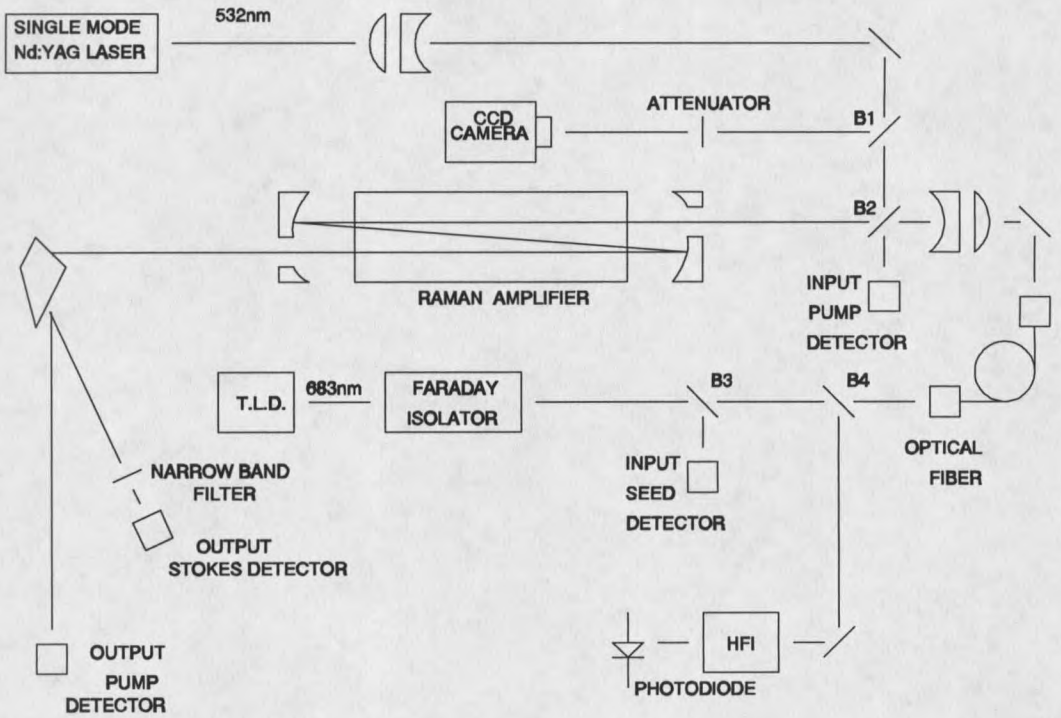


Figure 12 Experimental setup used to study the growth of an injection seeded Raman amplifier.

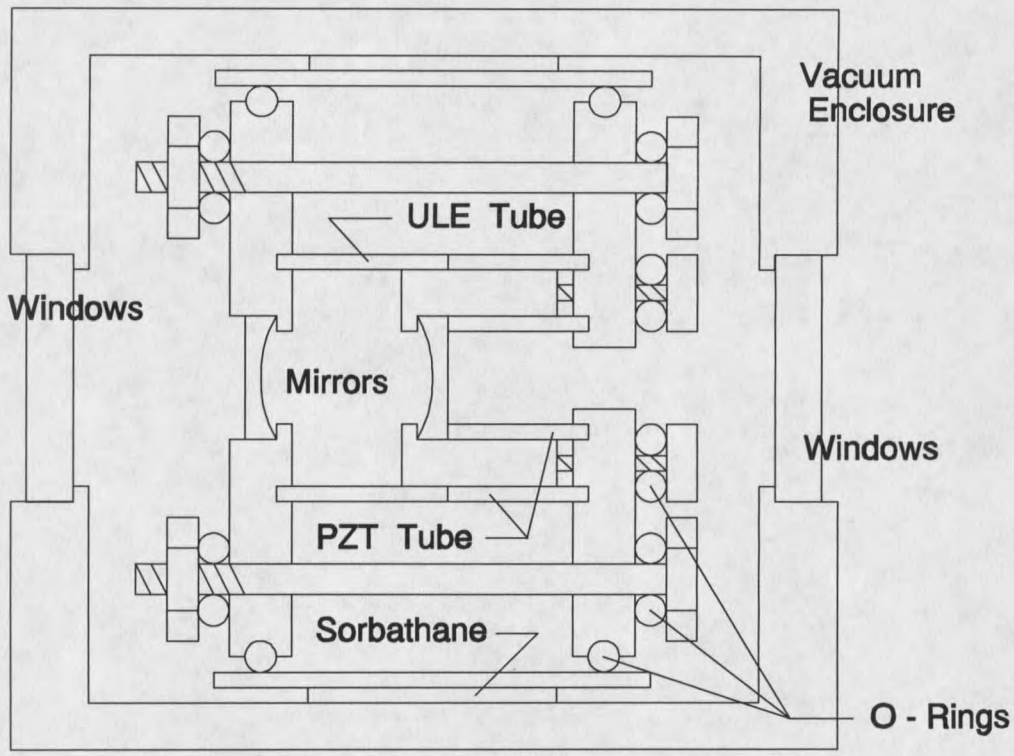


Figure 13 Schematic of the high finesse interferometer used in the seeding experiments.

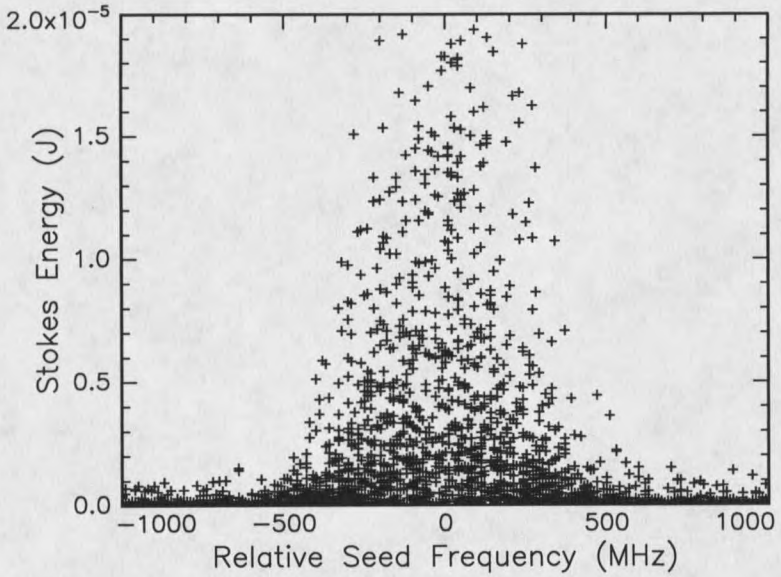


Figure 14 Output Stokes energy as a function of the relative seed frequency for input pump energies of 153±15μJ and input pump beam position (at focus) fluctuations of ±50μm. A total of 1500 shots were taken.

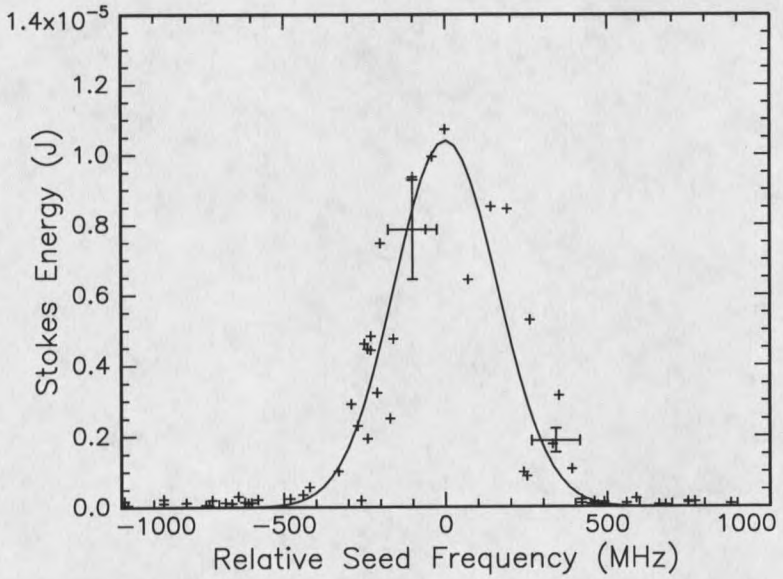


Figure 15 Same as figure 14 except the pump energy is 153±1μJ and the pump beam pointing fluctuations within an 11μmx13μm window. The solid curve is a least squares fit to the data.

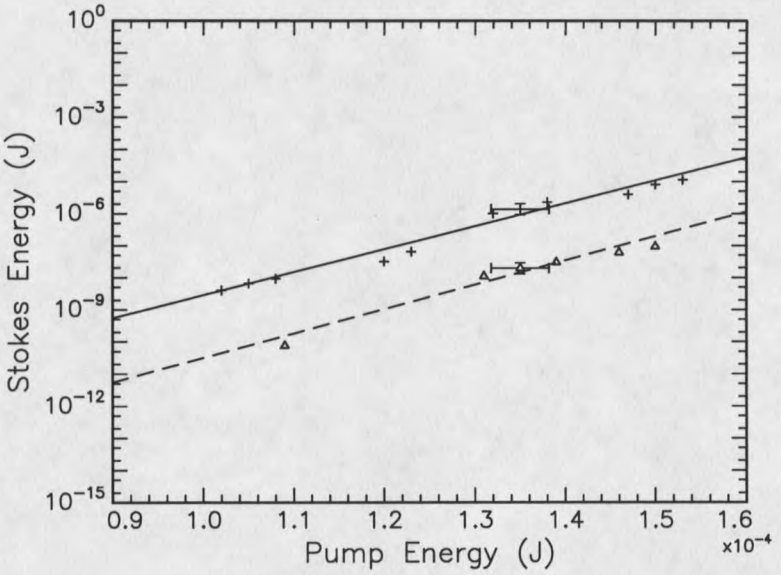


Figure 16 Output Stokes energy as a function on input pump energy after input pump energy and pointing fluctuations have been folded out. The solid line represents the predicted growth of the Stokes field for an input Stokes signal and the dashed line represents the predicted growth from spontaneous emission.

CHAPTER 5

SPATIAL STRUCTURE OF THE AMPLIFIED STOKES FIELD

Introduction

Understanding the spatial structure of the amplified field in an optical amplifier is critical in understanding how to optimize the performance of an optical amplifier. The two effects that are considered in this thesis which affect the spatial structure of the amplified field in an optical amplifier are index and gain guiding. As stated earlier, index and gain guiding can occur whenever the amplified gain is nonuniform in the transverse direction. Nonuniform gain in the transverse direction occurs when the amplifier is pumped by a beam whose intensity varies in the transverse direction. A common example for the Raman amplifier occurs when the Raman medium is pumped by a focused gaussian beam. However, the pumping of a optical amplifier by a focused gaussian is a very ubiquitous situation in optics so the results shown here should have a wide range of application.

The gain and index guiding effects on the spatial structure of the amplified Stokes beam are experimentally studied in this chapter. The description of the Raman amplifier, which usually includes only the imaginary part of the Raman susceptibility, does not match the measured values of the radius as the input Stokes signal is tuned across the Raman resonance. Including the total Raman susceptibility, which allows for both gain and index guiding, agrees with the experimental results and clearly demonstrates the need to include index guiding when describing optical amplifiers.

Spatial Structure Experiment

The experimental setup which allows the study of gain and index guiding as a function of the detuning Δ is shown in Fig.17. The pump beam is provided by a frequency doubled output at 532nm of an injection seeded Nd:YAG laser. The output of the Nd:YAG laser is reflected from an off axis spherical mirror to correct a slight astigmatism[47] present in the output of the Nd:YAG laser. The beam is then spatially filtered by a series of two pinholes[47] (not shown in Fig.17). The pump beam next passes through a series of two lenses which focus the pump beam at the center of the Raman amplifier. After the lenses, the pump beam impinges on a dichroic mirror labeled B1 in Fig.17. Part of the pump beam passes through B1 and is incident on the silicon energy detector which allows the monitoring of the pump energy for each shot of the pump laser. The rest of the pump beam is directed into the Raman amplifier.

The input Stokes signal is provided by a tunable laser diode (TLD) with a center frequency of 683nm. The output of the TLD is sent through a Faraday isolator which prevents feedback from affecting the performance of the TLD. The input Stokes signal is next incident on a beam splitter B2. Part of the input Stokes signal is sent via a single mode optical fiber to a HFI which is described in the previous chapter. The HFI allows us to accurately monitor the relative frequency of the input Stokes signal with sub MHz resolution. The remainder of the input Stokes signal is launched into a single mode optical fiber which provides a spatial filter for the input Stokes signal. The input signal then passes through a series of two lenses which allow the input Stokes to focus at the center of the Raman amplifier.

The input Stokes beam is combined with the pump beam at B1 and sent collinearly through a Raman amplifier which consists of H_2 at a pressure of 65atm. The higher pressure was used in this experiment because calculations indicate the shift away from the Raman resonance is larger at higher pressures. Both the pump and input Stokes signal make a single pass through a 141cm long Raman cell with both beams focusing at the center of the cell. The measured Rayleigh range of the input Stokes signal was 31.4cm and the measured Rayleigh range of the pump beam was 27.4cm.

After exiting the Raman amplifier, the pump and amplified Stokes signal pass through a lens with a focal length of 100cm which allows the Stokes beam at the exit of the Raman amplifier to be imaged onto a CCD camera with a measured magnification of 1.6. After the imaging lens , the pump beam is blocked using a dielectric mirror which

reflects the 532nm pump beam but allows the 683nm Stokes signal to pass. A narrow band interference filter centered at 680nm was placed behind the dielectric mirror to block any 532nm light that may have leaked through the dielectric mirror. This method of separating the pump beam and amplified Stokes beam was found to be superior to using a Pelin-Broca prism which introduced a significant astigmatism into the amplified Stokes beam. After the narrow band filter, the amplified Stokes beam is incident on beamsplitter B3. Part of the amplified Stokes signal is sent to a silicon energy detector which allows the energy of the amplified Stokes signal to be monitored. The remainder of the amplified Stokes signal is incident on a Pulinx TM-745 CCD camera . The CCD camera allowed the monitoring of the radius of the amplified Stokes signal with the aid of a commercially available beam profile program.

Data was taken as follows. The TLD was slowly tuned across the Raman resonance. The pump energy, relative input Stokes frequency, amplified Stokes signal energy, and amplified Stokes signal radius were monitored and recorded using a personal computer for each shot of the pump laser. The pump energy was set at 890 μJ which corresponds to a gain of G=6.65 where $\alpha = 2.95 \times 10^{-9}$cm/W[34] was used. The Raman linewidth was measured at 2880MHz which agreed with the published value for the Raman linewidth[31] at the pressure of 65atm which was used in this experiment.

Results

Numerical calculations which solve the wave equation by expanding the Stokes field over the nonorthogonal modal basis were performed for two cases. The first case includes the imaginary part of the Raman susceptibility only. In this case only gain guiding is allowed to occur. In the second case the total Raman susceptibility is included and both gain and index guiding are occurring. Figure 18 is a plot of the radius calculated for the amplified Stokes beam at the exit of the Raman amplifier as a function of the detuning Δ.

The dashed line is the result of solving the wave equation for case 1 in which only gain guiding is occurring. At $\Delta=0$, the radius of the amplified Stokes beam at the exit of the Raman amplifier is a minimum. At $\Delta=0$, the gain $(g(z,r_T)\frac{\Gamma^2}{\Delta^2+\Gamma^2})$ is a maximum and the gain guiding effect which acts to narrow the Stokes beam is the strongest. As Δ is detuned away from the Raman resonance the gain decreases and the gain guiding narrows the amplified Stokes beam less. At large detunings , the gain goes toward zero and the radius of the Stokes beam approaches the radius of the input signal.

The solid line in Fig.18 is the result of solving the wave equation when the total Raman susceptibility is included in the wave equation. Both gain and index guiding are occurring in this case. For $\Delta>0$ ($\Delta<0$) notice that the radius of the amplified Stokes beam is smaller (larger) than gain guiding predicts. The additional narrowing of the amplified Stokes beam results from index guiding. The index guiding is related to the

real part of the Raman susceptibility and is proportional to $g(z,r_T)\frac{\Gamma\Delta}{\Delta^2+\Gamma^2}$. At $\Delta>0$ ($\Delta<0$), index guiding acts as a focusing (defocusing) lens which focuses (defocuses) the amplified Stokes beam to a smaller (larger) spot size.

Figure 19 shows the correlation of the change in radius of the amplified Stokes beam as a function of detuning as the solid line with the change in the real part of the Raman susceptibility. The real term of the Raman susceptibility, which leads to index guiding, is shown in Fig.19 as the dashed line. The strength of the index guiding is proportional to the magnitude of the real part of the Raman susceptibility. The minimum radius for the amplified Stokes beam occurs when the real part of the Raman susceptibility is a maximum at Δ=1440MHz. When $\Delta>0$ the real part of the Raman susceptibility acts to focus the amplified Stokes. For $\Delta<0$ the real part of the Raman susceptibility acts to defocus the amplified Stokes beam. At $\Delta<$-1200MHz, the Stokes radius has become large enough so that only a small percentage of the amplified Stokes overlaps the gain profile and hence the Stokes experiences a very weak gain.

Figure 20 is a plot of the normalized Stokes energy as a function of detuning Δ. The +'s represent experimental data taken by scanning the TLD across the Raman resonance. The dashed line is a least squares fit to the data and the solid line is the theoretical result from solving the wave equation. The on resonance case occurs when Δ=0MHz. Notice that the peak Stokes output is shifted to the blue side of the Raman resonance. The shift results from focusing of the amplified Stokes due to index guiding. The peak Stokes output occurs at Δ=230MHz and results from competition between an

increase in gain due to a narrower Stokes beam which is caused by index guiding and a loss in gain due to the detuning[24]. This will be studied in more detail in the next chapter.

The Raman resonance at Δ=0MHz was determined experimentally as follows. The shift in the peak Stokes is a function of the gain of the Raman amplifier[24]. As the gain is lowered, the index effect has a smaller focusing effect on the amplified Stokes beam and hence the increase in the gain due to a narrower Stokes beam overlapping a more intense part of the pump beam becomes negligible. At low gains the peak of the Stokes output occurs at $\Delta \approx 0$ MHz. Experimentally, the gain was lowered by lowering the pump energy and the TLD was swept across the Raman resonance to find $\Delta \approx 0$ MHz. An experiment is presented in the next chapter which will show the detuning which yields the peak Stokes output as a function of gain.

Figure 21 shows the radius of the amplified Stokes beam at the exit of the Raman amplifier as a function of the detuning. The solid and dashed lines are the same as in Fig.18 and the +'s are the experimental points. The detuning range was limited in the experiment to approximately 1000MHz where the gain was large enough for the CCD camera to measure the amplified Stokes beam. Beyond this detuning range, the gain was too small so that the CCD camera could not measure the amplified Stokes beam. Each experimental point consists of an average of at least 25 pump shots within a frequency window of 40MHz. The measurements clearly indicate that both gain and index guiding are needed to account for the change in the Stokes radius in the Raman amplifier as the detuning is varied.

The experimental results show that the radius of the amplified Stokes beam decreases as the input Stokes signal is detuned to the blue side of the Raman resonance. This result does not agree with the predictions of theories which include only the imaginary part of the Raman susceptibility and allow only for gain guiding. When the total Raman susceptibility is included which allows both gain and index guiding in the theory, the theory accurately predicts the results.

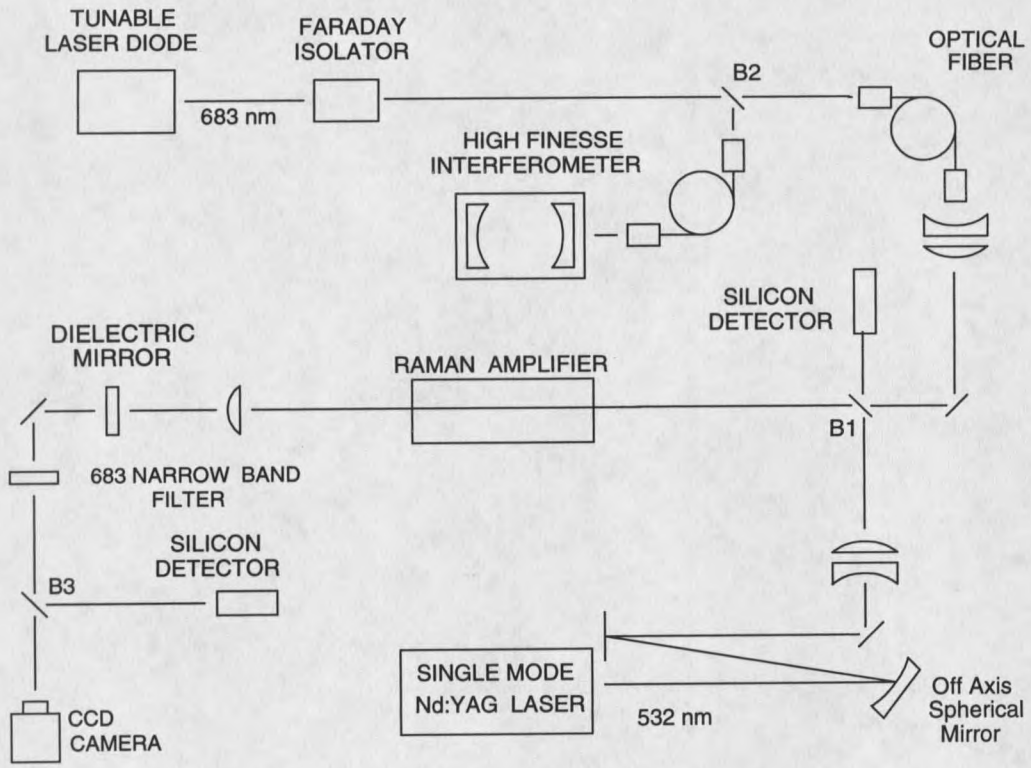


Figure 17 Schematic of the experimental setup which is used to measure the radius of the amplified Stokes at 683nm as a function of the detuning from the Raman resonance of the input Stokes signal.

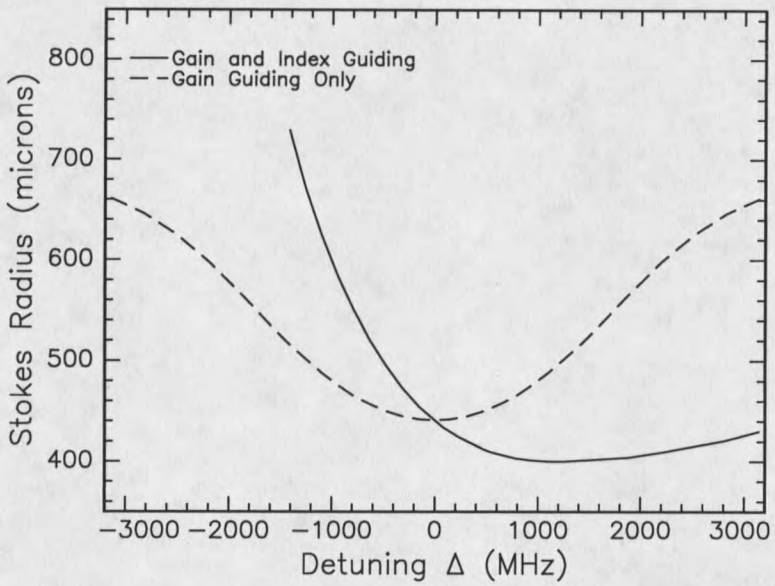


Figure 18 A plot of the radius of the amplified Stokes beam as a function of detuning Δ. The dashed line represents the case where only gain guiding was included. The solid line represents the case where both gain and index guiding were included. The radius of the solid line reaches a minimum at Δ=1400MHz while the minimum of the dashed line is Δ=0MHz.

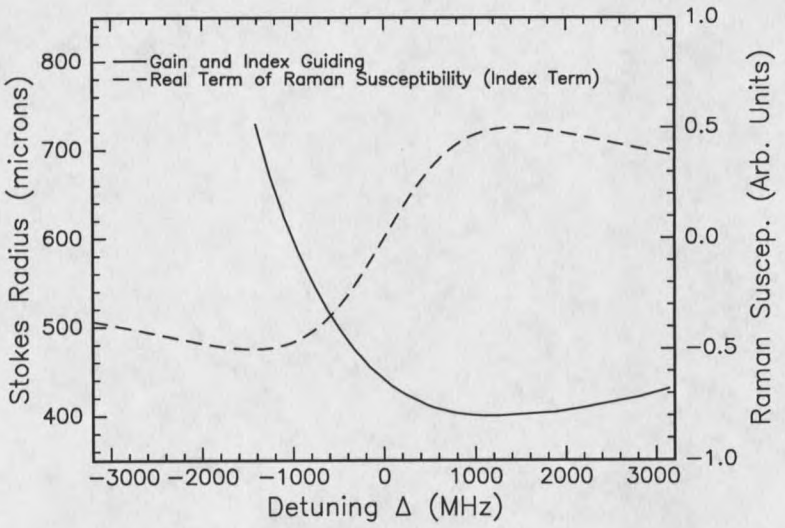


Figure 19 The solid line is the same as in Figure 18. The dashed line represents the real part of the Raman susceptibility. Notice that the minimum radius of the amplified Stokes beam occurs when the real part of the Raman susceptibility is a maximum. For $\Delta>0$ ($\Delta<0$) the real part of the Raman susceptibility acts as a focusing (defocusing) lens.

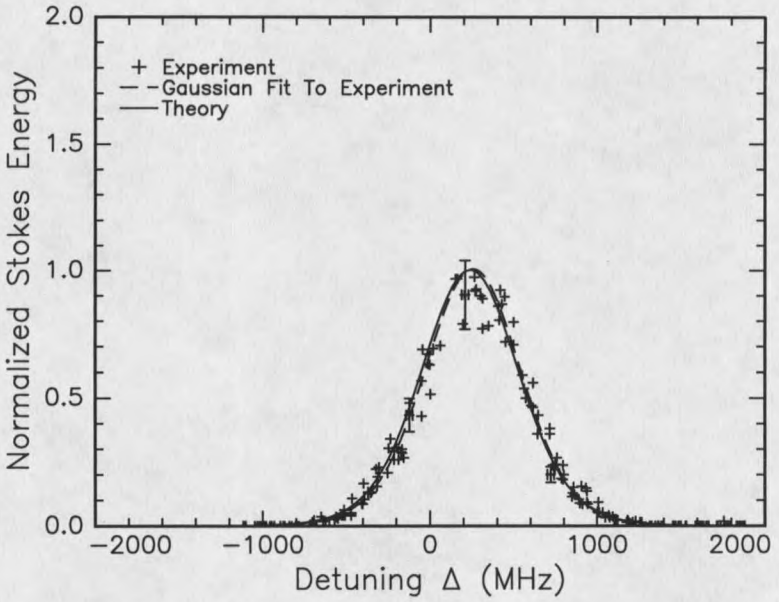


Figure 20 A plot of the normalized Stokes output energy as a function of detuning from the Raman resonance. The +'s correspond to experimental data, the dashed line is a gaussain least squares fit to the data, and the solid line is the theoretical predictions from solving the wave equation using a nonorthogonal modal expansion for the Stokes field. The on resonance case (Δ=0MHz) was determined by lowering the gain which causes the peak Stokes output to move toward Δ=0MHz. Notice that the peak Stokes output is not at Δ=0MHz but is shifted towards the blue side of the Raman resonance by Δ=230MHz.

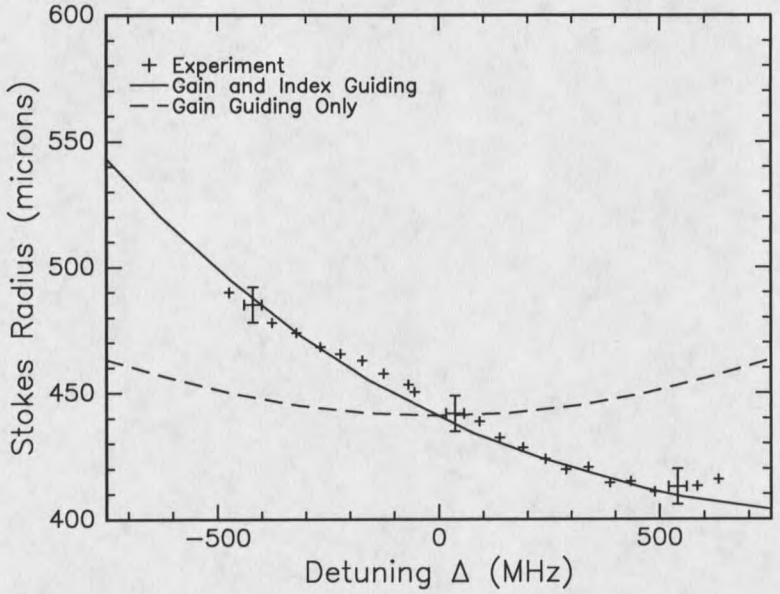


Figure 21 A plot of the radius of the amplified Stokes beam at the exit of the Raman amplifier. The dashed and solid line are the same as in figure 18. The +'s represent experimental measurements. The experimental measurements are in agreement with the predictions of the wave equation when the total Raman susceptibility is included in the wave equation allowing for gain and index guiding.

CHAPTER 6

FREQUENCY ASYMMETRIC GAIN PROFILE IN A SEEDED RAMAN AMPLIFIER

Introduction

As alluded to in the previous chapter, the peak Stokes output of a Raman amplifier does not occur at the Raman resonance but rather when the input Stokes signal is detuned to the blue side of the Raman resonance. In the simplest sense this phenomena can be explained as follows. The real part of the Raman susceptibility, which depends on the pump intensity, manifests itself as a index of refraction and can be thought of as creating a lens which can focus or defocus the amplified Stokes beam depending on which side of the Raman resonance the input Stokes signal is tuned to. The focusing effect was measured in the previous chapter. On the blue side of the Raman resonance, the amplified Stokes beam will be focused to a smaller spot size. which leads to higher output Stokes energy. This is because the smaller Stokes beam experiences a higher gain

as it spatially overlaps a more intense part of the pump beam which is proportional to the gain.

The output Stokes energy is numerically and experimentally studied as a function of detuning from the Raman resonance for a large range of gains. The peak Stokes output of the Raman amplifier occurs not at the Raman resonance as might be expected but occurs when the input Stokes signal is shifted to the blue side of the Raman resonance. This result is not explained by the previous theories of Raman scattering that include only the imaginary part of the Raman susceptibility and only allow for gain guiding. This result however is predicted when the total Raman susceptibility is included in the wave equation which allows for gain and index guiding.

Frequency Dependence Of The Stokes Output

In this section the output Stokes energy is calculated as a function of the detuning of an input seed for typical experimental parameters appropriate for vibrational Raman scattering in H_2 with a pump laser at 532nm, and a input Stokes signal tuned near the Raman resonance at 683nm. It should be noted that the parameters used in this section correspond to the experimental parameters that will be discussed later in this chapter. Also, the parameters used in this chapter are different than those used in the previous chapter. The length of the gain medium is 141cm, and the Rayleigh range of the focused gaussian pump beam is 30cm. The input to the Raman amplifier is at z=-70cm which corresponds to θ_{in}=-1.17 and the output is at z=70 which corresponds to θ=1.17. The

plane wave gain coefficient $\alpha = 2.94 \times 10^{-9}$cm/W[34] and the Raman linewidth of $\Gamma = 3200$MHz[31] are used for the following calculations.

Figure 22 shows a plot of the output Stokes energy as a function of detuning for G=0.5, G=1, and G=4. The dashed line is the predicted Stokes output energy as a function of detuning when the real part of the Raman susceptibility is not included in the wave equation. The solid line represents the predicted output Stokes energy as a function of detuning when the total Raman susceptibility is included in the wave equation. The output Stokes energy is normalized to the maximum output Stokes energy when the real part of the Raman susceptibility is not included in the wave equation. For G=0.5 including the real part of the Raman susceptibility makes little difference in the output Stokes energy. However at G=1 the peak Stokes output energy is shifted to the blue side of the Raman resonance by 186MHz. At G=4 this effect is even more pronounced with the peak output Stokes energy shifted to the blue side of the Raman resonance by 306MHz and the peak Stokes energy is increased by 25% compared to the peak Stokes energy predicted when only the imaginary part of the Raman susceptibility is included in the wave equation. The focusing effect, which was studied in the last chapter, is responsible for this shift in the peak Stokes output energy. The increased peak Stokes energy on the blue side of the Raman resonance can be explained by realizing that the focusing effect causes the amplified Stokes signal to spatially overlap a higher gain in the Raman active medium.

The gain narrowing of the Raman linewidth has been studied in the literature and allows us to compare the linewidths calculated in this thesis with previous results. The HWHM linewidth predicted by Ref.46 is

$$\Delta\nu = \frac{\Gamma}{\sqrt{4\mu G\theta - 1}} \qquad 6.1$$

where the results of Ref.29,33 have been used to rewrite Eq.6.1. For G=5 and μ=.438, Eq.6.1 predicts a HWHM of 438MHz. Figure 23 is a plot of the calculated normalized Stokes energy as a function of detuning for G=5. The circles denote the calculated values for the Stokes energy at different detunings. The solid line is a least squares fit to the calculated data. The HWHM of the least squares fit is 453MHz which compares favorable with the result from Eq.6.1.

Figure 23 shows, as a function of gain, the detuning from the Raman resonance that leads to the maximum output Stokes energy. This plot emphasizes the dramatic shift from the Raman resonance that is caused by the index guiding. The detuning at which the peak Stokes output occurs reaches a maximum at about G=4 and then starts to fall off as the gain is further increased. This reversal at high gain can be explained as follows. The focusing caused by the real part of the Raman susceptibility on the blue side of the Raman resonance causes the Stokes beam to spatially overlap a higher gain region. However once the Stokes beam is narrow compared to the pump beam, the entire Stokes beam experiences essentially the on-axis gain. Further increase in G has little effect on the

Stokes field. On the other hand the Stokes (frequency) gain profile, due to the imaginary part of the Raman susceptibility, becomes narrower without bound as G is made larger. The net result is that at large G the index guiding which leads to larger Stokes output energy at high detunings can no longer compensate for the spectral gain narrowing and the peak location starts to move back towards the Raman resonance.

Experiment

The experimental apparatus to probe the effects of pump energy and detuning on the Stokes output is shown in Fig.25. The experimental apparatus is similar to that of the previous chapter up to the beam combiner B1 shown in Fig25 and Fig.17 and this part of the experimental description will not be repeated here. The experimental set varies after B1 and is described below.

After the beam combiner B1 the input Stokes signal and pump beam travel conlinearly through the Raman amplifier. The Raman amplifier consists of H_2 at a pressure of 70atm. The Raman amplifier is a 141cm in length and the pump and Stokes make a single pass. The Rayleigh range of the both the pump and input Stokes signal was 30cm.

The pump and amplified Stokes pass through two Pelin-Broca prisms that separate the pump and Stokes beams. The Stokes beam is split at beam splitter B3 with part of the beam traveling to a Si energy detector and part of the beam traveling to a photomultiplier tube (PMT). The PMT is calibrated to the absolute energy of the Si

energy detector with the aid of neutral density filters. This detection scheme allows for a large dynamic range of output Stokes energy to be measured.

Data is collected as follows. At a particular pump energy, the TLD is scanned across the Raman resonance. As the TLD is scanned the input pump energy, relative input Stokes frequency, and output Stokes energy is recorded via a personal computer for each shot of the pump laser. A total of 1200 shots are collected at each pump energy. A scan across the Raman resonance at a reference pump energy is run after each different pump energy. The scan at the reference pump energy allows monitoring of the HFI to ensure that it is not drifting during the experiment.

Experimental Results

Figure 26 shows the results of a scan across the Raman resonance for a pump energy of 545 μJ (G=3.44). The +'s correspond to the experimentally measured output Stokes energy as the TLD was swept across the Raman resonance. The zero detuning point was determined from the data shown in Fig.27. The solid line is the calculated output Stokes as a function of detuning which results from solving the wave equation and the dashed line is a least squares fit to the data. The linewidth from the least squares fit is 551MHz while the linewidth from the calculations is 591MHz. These linewidths can be compared to the gain narrowed linewidth predict by Eq.6.1 which is 542MHz. The measured and calculated linewidth compare favorably with the gain narrowed linewidth.

Figure 27 is a plot of the detuning that gives the maximum Stokes output as a function of G. The +'s represent experimentally measured values while the solid line represents the theoretical calculations. Because the frequency measurement is a relative measurement, all the data is shifted to match the theoretical curve in Fig.27. This is how the zero detuning was determined for the experimental frequency measurements shown in Fig.26 and for the experimental results presented in the previous chapter. For G in the range 0 to 4 the detuning which gives the peak Stokes output increases as the gain increases. For G>4 the detuning which gives the maximum Stokes output begins to fall off as discussed previously in this chapter.

The experiment clearly shows that substantial index guiding is occurring in a gain guided Raman amplifier. Index guiding effects can cause some rather unexpected results such as the shift away from the Raman resonance by over 300MHz for the peak output Stokes energy. The fact that index guiding is occurring in a gain and index guided Raman amplifier implies that the spatial structure of the amplified Stokes signal results from a complicated interaction of the Stokes field with the pump beam through the Raman susceptibility and index guiding effects need to be carefully considered in optical systems.

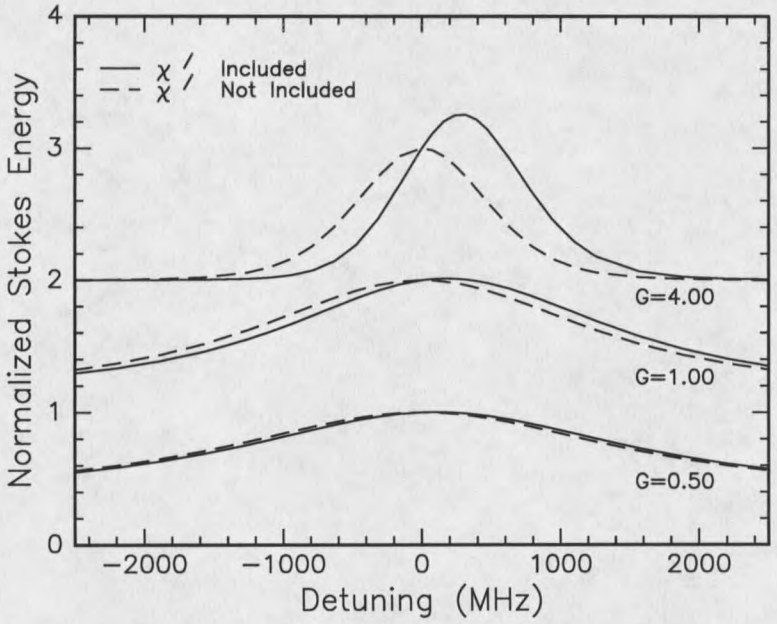


Figure 22 Normalized Stokes energy as a function of detuning from the Raman resonance for G=0.5, G=1 and G=4. The solid line represents calculations done with χ' included in the theory while the dashed line represents calculations done with χ' not included in the theory. The output for each gain has been normalized so that the peak output Stokes energy is unity when χ' is not included in the theory. For G=1, the output Stokes has been shifted up by 1 and for G=4, the output Stokes energy has been shifted up by 2. As G is increased, the peak of the output Stokes energy shifts in frequency and increases in magnitude.

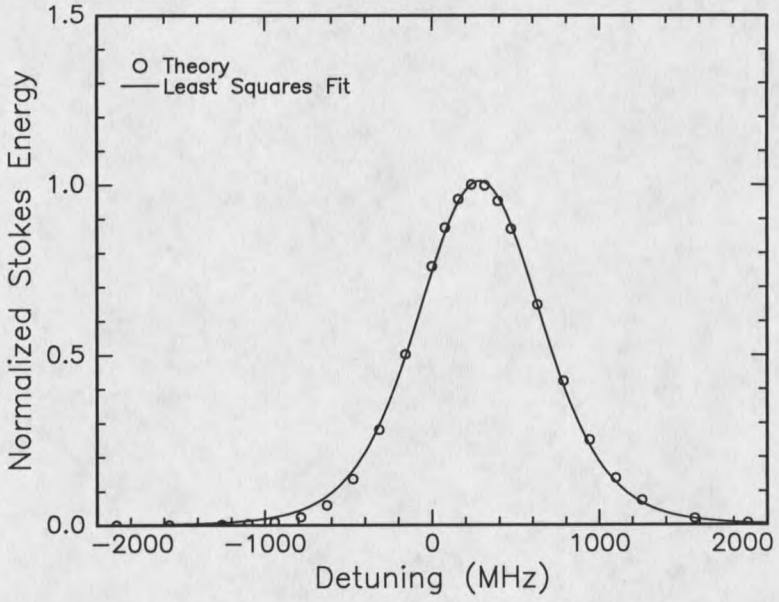


Figure 23 Normalized Stokes output as a function of detuning from the Raman resonance for G=5. The circles represent numerical calculations while the solid line is a gaussian fit to the calculated results. The output Stokes energy is a gaussian and the linewidth compares favorably to the gain narrowed linewidths of previous work [15].

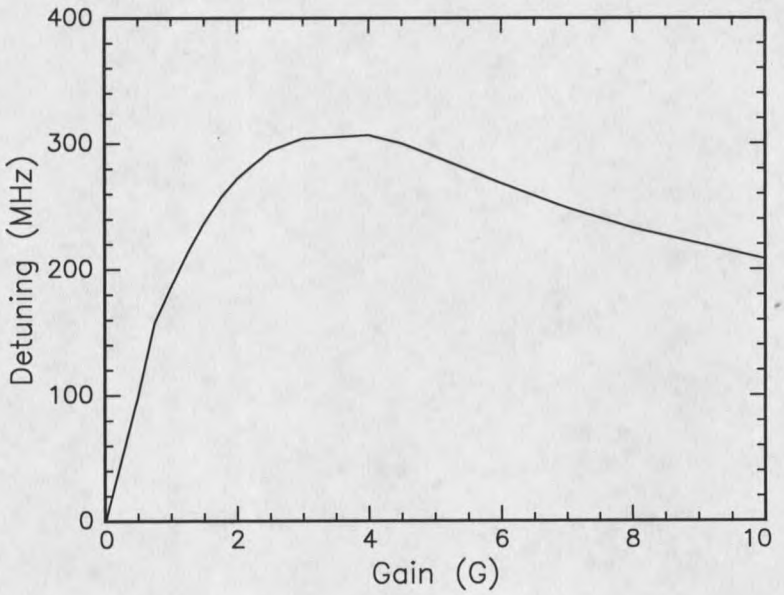


Figure 24 The detuning from the Raman resonance that gives the peak Stokes output energy as a function of the gain G. The maximum detuning of 306MHz is reached for G=4. At higher gains, the pump induced focusing, which leads to larger Stokes output at high detuning can no longer compensate for the spectral gain narrowing and the peak Stokes energy starts to move back towards the Raman resonance.

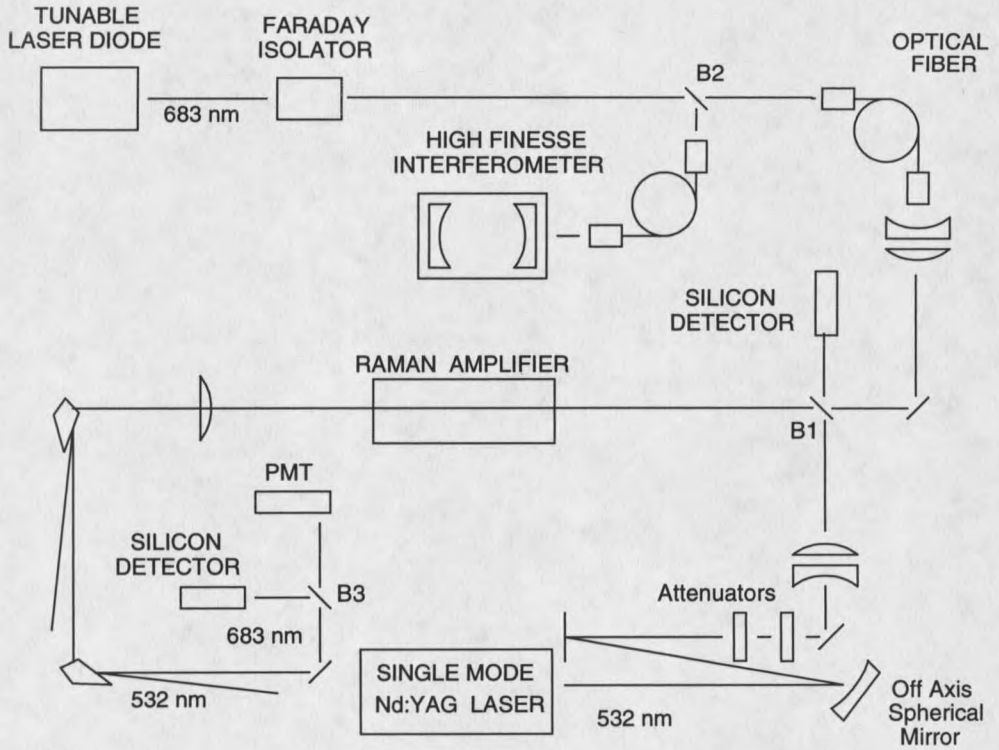


Figure 25 Experimental apparatus used to study index guiding effects in a gain-guided Raman amplifier.

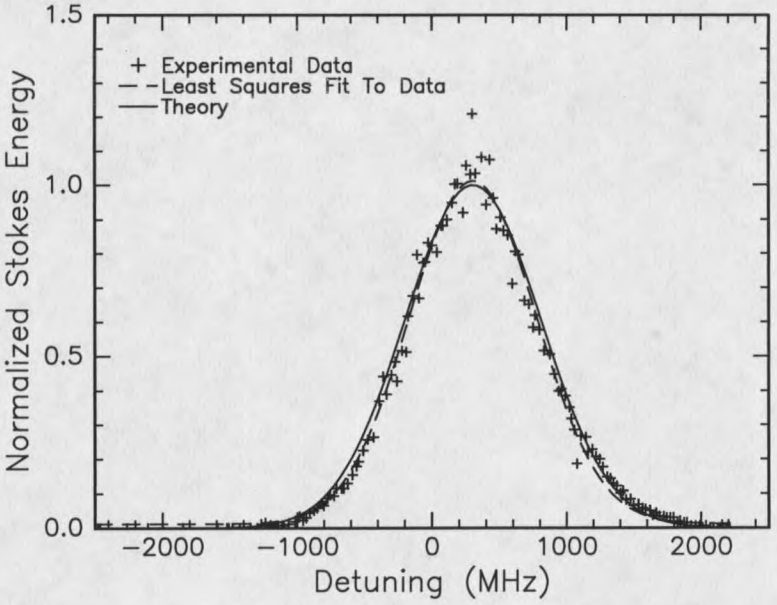


Figure 26 Normalized output Stokes energy as a function of relative seed frequency. The +'s are experimental points for a gain G=3.44. The dashed line is a gaussian least squares fit to the data points. The solid line is the prediction from solving the Maxwell wave equation using a Gauss Laguerre expansion for the Stokes field. The maximum output occurs when the input seed is tuned over 300MHz to the blue side of the Raman resonance.

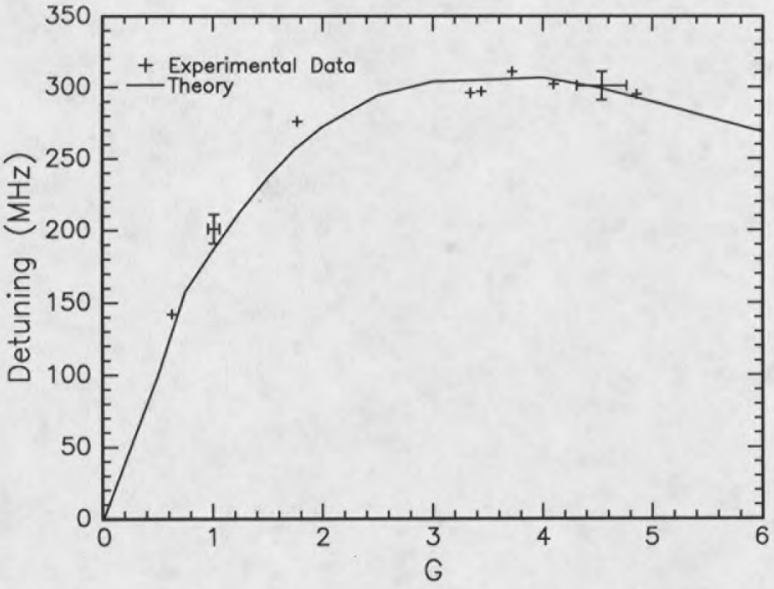


Figure 27 Detuning which gives the maximum Stokes output as a function of gain. The +'s are the measured shift of the peak Stokes output while the solid line is the prediction from solving the Maxwell wave equation by expanding the Stokes field over a Gauss Laguerre basis. At low gains the effect of index guiding is minimal and the maximum Stokes output occurs at a detuning of zero. At higher gains the peak Stokes output is shifted to the blue side of the Raman resonance.

CHAPTER 7

CONCLUSION

Summary

In chapter two, a model for the Raman susceptibility was presented which led to an equation for the Raman susceptibility. The Raman susceptibility was included in the wave equation and the wave equation was solved by expanding the amplified Stokes field over two different bases. Two different bases were used in the Stokes field expansion, and the choice of the basis depends on whether one wishes to describe the input Stokes signal or the amplified Stokes signal in terms of a single mode. The nonorthogonal modal expansion is useful for describing the amplified Stokes field with a single mode but describing the input Stokes signal is not easy. The Gauss-Laguerre basis needs many modes to describe the amplified Stokes field but only a single mode is needed to describe the input Stokes signal. The Gauss-Laguerre basis is much easier to use to describe more complicated input Stokes signals such as a input Stokes signal with a phase shift that can

be used to look for dark soliton solutions. The reason for this is the orthonormal properties of the Gauss-Laguerre modes which do not hold for the nonorthogonal modes.

It was argued that the imaginary part of the Raman susceptibility leads to gain and gain guiding while the real part of the Raman susceptibility leads to an index of refraction and index guiding. Both gain and index guiding affect the spatial structure of the amplified Stokes beam. The gain guiding acts to narrow the amplified Stokes beam while index guiding can either narrow or widen the Stokes beam. The spatial structure of the amplified Stokes beam results from a complex interplay of the gain and index guiding and the detuning Δ. The phasefronts of the amplified Stokes field are very complicated as seen in chapter three and an understanding of these phasefronts can be used to enhance the performance of the Raman amplifier.

Index guiding effects complicate the use of the Raman amplifier. The maximum gain is no longer at the Raman resonance as one would expect but rather occurs when the input Stokes signal is tuned to the blue side of the Raman resonance. This result was not predicted by previous work in gain guided amplifiers where only the imaginary part of the Raman susceptibility was included in the wave equation. The shift of the peak output Stokes energy from a Raman amplifier is attributed to the fact that the index effect focuses the amplified Stokes beam when the input Stokes is tuned to the blue side of the Raman resonance. The focused Stokes beam experiences a higher gain because the smaller spot size overlaps a more intense part of the pump beam and hence experiences a larger gain. The focusing of the Stokes beam caused by the real part of the Raman

susceptibility was measured in another experiment. The results of this experiment contradict the predictions of previous theories of Raman scattering where only the imaginary part of the Raman susceptibility was included in the wave equation. The experimental results were in agreement with the predictions of the wave equation when both gain and index guiding were included thus showing again the need to consider index guiding when working with optical amplifiers.

Future

As is the case in science, this research has answered questions about the spatial structure of the amplified field in a gain and index guided optical amplifier and opens the door to several other questions. One particular question I would like to present for future work is the possibility to use gain and index guiding to create bright or dark spatial solitons in a gas, something which to my knowledge has not been mentioned in the literature.

The photorefractive effect[48,49] has been used to modify the spatial structure of a beam propagating through a crystal. This effect can be used to compensate for the effects of diffraction and allow the beam to propagate without changing its radius. The gain and index effects can also be used to compensate for diffraction in a Raman amplifier. However, no amplifier parameters have been found yet that lead to an amplified Stokes beam which propagates with the gain and index effects exactly compensating for diffraction.

REFERENCES CITED

REFERENCES CITED

1. A. Yariv, **Quantum Electronics 3rd Edition**, (John wiley and Sons, New York, 1989).
2. H Rabin, C. Tang, **Quantum Electronics Volume 1, Nonlinerar Optics Part A**, Academic Press, New York, 1975).
3. D. Long, **Raman Spectroscopy**, (McGraw Hill Internation Book Company, New York, 1977).
4. N. Bloemberg, Amer. J. of Physics **35** ,989, (1967).
5. J. Ducuing and F. de Martini, Phys. Rev. Lett **17**, 117, (1966).
6. M. Abraham, F. Arecchi, A. Mooradian, and A. Sona**, Physics of New Laser Sources**, (Plenum Press, New York, 1985).
7. H. Komine and E.A. Stappaerts, Opt. Lett **4**, 398, (1979).
8. F.Y.F Chu and A.C. Scott, Phys. Rev. A **12**, 2060, (1975).
9. K. Druhl and G. Alsing, Physica D **20**,429, (1986).
10. C.R. Menyuk, Phys.Rev Lett. **62**, 2937, (1989).
11. D.C. MacPherson, J.L. Carlsten, and K. Druhl, J. Opt. Soc. Am. B **4**, 1853, (1987).
12 J.W. Haus and M. Scalora, Phys. Rev A **42**, 3149, (1990).

13. D.C. MacPherson, R.C. Swanson, and J.L. Carlsten, Phys. Rev A **39**, 6078, (1989).

14. R.C. Swanson, D.C. MacPherson, P.R. Battle and J.L. Carlsten, Phys. Rev. A **45**, 450, (1990).

15. R.C. Swanson, P.R. Battle, and J.L. Carlsten, Phys. Rev. Lett. **67**, 38, (1991).

16. R.C. Swanson, P.R. Battle, and J.L. Carlsten, Phys. Rev. A **44**, 1922, (1991).

17. H.A. Haus and S. Kawakami, IEEE J. Of Quantum Electron. **21**, 63, (1985).

18. A.E. Siegman, Phys. Rev. A **39**, 1253, (1989).

19. P.R. Battle, J.G. Wessel, and J.L. Carlsten, Phys. Rev A **48**, 707, (1993).

20. S.J. Kuo, D.T. Smithey, and M.G. Raymer, Phys. Rev. Lett. **20**,2605, (1991).

21. Pamendt, R.A. London, and M. Strauss, Phys. Rev. A **44**, 7478, (1991).

22. I.H. Deutsch, J.C. Garrison, and E.M. Wright, J. Opt. Soc. Am. B **8**, 1244, (1991).

23. K.S. Repasky, J.K. Brasseur, and J.L. Carlsten, "Spatial Structure of the Amplified Stokes Field in a Gain and Index Guided Raman Amplifier", Submitted to Phys. Rev. A, (1996).

24. K.S. Repasky and J.L. Carlsten, "Frequency Asymmetric Gain Profile in a Seeded Raman Amplifier", Accepted for publication in Phys. Rev. A, (1996).

25. K. Peterman, IEEE J. of Quantum Electron. **QE-15**, 566, (1979).

26. J. Mostowski and B. Sobolewska, Phys. Rev A **34**, 3109, (1986).

27. B.N. Perry, P. Rabinowitz, and M. Newstein, Phys. Rev. A **27**,1989, (1983).

28. B.N. Perry, P. Rabinowitz, and D.S. Bomse, Opt. Lett. **10**, 146, (1985).

29. D.C. MacPherson, R.C. Swanson, and J.L. Carlsten, IEEE J. of Quantum Electron.

25, 1741, (1989).

30. .G. Wessel, K.S. Repasky, and J.L. Carlsten, Opt. Lett. **19**, 1430, (1994).

31. W.K. Bischel, and M.J. Dyer, Phys. Rev. A **33**, 3113, (1986).

32. J.G. Wessel, P.R. Battle, and J.L. Carlsten, Phys. Rev. A **3**, 2587, (1994).

33. The gain coefficient G can be related to parameters that are typical in Raman amplifier experiments as $G = \alpha P_p / \lambda_g$ where α is the plane wave gain coefficient[34], P_p is the peak pump power, and λ_g is the wavelength of the pump laser.

34. W.K. Bischel and M.J. Dyer, J Opt. Soc. Am. B **3**, 677, (1986).

35. J.G. Wessel, K.S. Repasky, and J.L. Carlsten, "Enhanced coupling into a Gain Guided Amplifier", accepted for publication in Phys. Rev. A, (1996).

36. R.C. Swanson, P.R. Battle, and J.L. Carlsten, Phys. Rev. A **45**, 1932, (1992).

37. M.D. Duncan, R. Mahon, L.L. Tankersley, and J. Reintjes, J.Opt. Soc. Am B **9**, 2107, (1992).

38. I.A. Wamsley and M.G. Raymer, Phys. Rev. Lett. **50**, 962, (1983).

39. D.C. MacPherson, R.C. Swanson, and J.L. Carlsten, Phys. Rev Lett. **61**, 66, (1988).

40. M.D. Duncan, R. Mahon, L.L. Tankersley, and J. Reintjes, J.Opt. Soc. Am. B **7**, 1336, (1990).

41. M. Uchida, M. Nagasaka, and H. Tashiro, Opt.Lett. **14**, 1350, (1989).

42. K.S. Repasky, L.E. Watson, and J.L. Carlsten, Appl. Opt. **34**, 2615, (1995).

43. K.S. Repasky, J.G. Wessel, and J.L. Carlsten, Appl. Opt. **35**, 609, (1996).

44. J.M. Vaughan, **The Fabry Perot Interferometer: History, Theory, Practice, and**

Application, (Hilger, London, 1989).

45. G. Hernadez, **Fabry Perot Interferometers**, (Cambridge U. Press, Cambridge, U.K., 1986).

46. M.G. Raymer and J. Mostowski, Phys. Rev A **24**, 1980, (1981).

47. K.S. Repasky, J.K. Brasseur, J.G. Wessel, and J.L. Carlsten, "Correcting an Astigmatic Non Gaussian Beam", accepted for publication in Appl. Opt. (1996).

48. M. Segev, B. Crosignami, and A. Yariv, Phys. Rev A **68**, 923, (1992).

49. G. Duree, G. Salamo, M. Sergev, A Yariv, B. Crosignami, P. DiPorto, and E. Sharp, Opt. Lett. **19**, 1195, (1994).

APPENDICES

APPENDIX A

THE WAVE EQUATION

The wave equation which describes the growth of the Stokes field in a Raman amplifier is derived in this section. The derivation is short but it is nice to include so that the approximations that are made are readily seen.

The starting point for the derivation of the wave equation are Maxwell's equations which are written in cgs units as

$$\nabla \cdot E_s = 4\pi\rho$$

$$\nabla x E_s = -\frac{1}{c}\frac{\partial B_s}{\partial t}$$

$$\nabla x B_s = \frac{1}{c}\frac{\partial D_s}{\partial t} \qquad \text{A.1}$$

$$D_s = (1 + 4\pi\chi_L)E_s + 4\pi\chi_{NL}\left|E_p\right|^2 E_s$$

where E_s (E_p) is the Stokes (pump) electric field, B_s is the Stokes magnetic field, D_s is the Stokes electric displacement field, ρ is the electric charge density, c is the speed of light, χ_L is the linear Raman susceptibility and χ_{NL} is the non linear susceptibility. Taking the curl of the first equation listed in Eq.A.1 and using the fact that $\nabla(\nabla \cdot E) = 0$ which results from the first equation listed in Eq.A.1 when ρ=0 allows us to write

$$\nabla^2 E = \frac{1}{c^2}\frac{\partial^2 E}{\partial t^2} + \frac{4\pi}{c^2}\chi_L\frac{\partial^2 E}{\partial t^2} + \frac{4\pi}{c^2}\chi_{NL}\left|E_p\right|^2\frac{\partial^2 E}{\partial t^2} \qquad \text{A.2}$$

The field is assumed to travel in the +z direction. The laplacian is broken up into two pieces and is written $\nabla^2 = \nabla_T^2 + \frac{\partial^2}{\partial z^2}$ where $\nabla_T^2 = \frac{\partial^2}{\partial x^2} + \frac{\partial^2}{\partial y^2}$ is defined as the transverse laplacian. The field in Eq.A.2 is written as $E_s(r,t) = \frac{1}{2} E_s(z,r_T) e^{i(\omega t - kz)} + c.c.$ where $E_s(z,r_T)$ is a slowly varying envelope, ω is the angular frequency that the field is oscillating at , and k is the wavevector of the field. Using this ansatz, invoking the slowly varying envelope approximation, $\frac{\partial^2 E(z,r_T)}{\partial z^2} << k \frac{\partial E(z,r_T)}{\partial z}$, and realizing that $\frac{\omega^2}{c^2}(1 + 4\pi\chi_L) = k^2$ allows Eq.A.2 to be written

$$\nabla_T^2 E(z,r_T) - 2ik\frac{\partial E(z,r_T)}{\partial z} = -\frac{4\pi\omega^2}{c^2}\chi_{NL}\left|E_p\right|^2 E_s(z,r_T) \qquad \text{A.3}$$

The transverse laplacian in Eq.A.3 allows for the transverse variations of the field. The second term in Eq.A.3 tells how the field grows as it propagates in the z direction and the last term allows for the gain and index guiding effects.

APPENDIX B

TRANSIENT STIMULATED RAMAN SCATTERING EQUATIONS

The equations which describe transient stimulated Raman scattering for plane wave excitation in the retarded time frame are[13]

$$\frac{\partial}{\partial z}E_p = -\beta Q E_s \qquad \text{B.1}$$

$$\frac{\partial}{\partial z}E_s = +\beta Q^* E_p \qquad \text{B.2}$$

$$\frac{\partial}{\partial \tau}Q^* = -(\Gamma + i\Delta)Q^* + E_p^* E_s \qquad \text{B.3}$$

where E_p (E_s) is the slowly varying envelope of the pump (Stokes) field oscillating at frequency ω_p (ω_s), τ is the retarded time given by $\tau = t - z/c$, z is the location in the Raman amplifier and Δ is the detuning given by $\Delta = \omega_v - (\omega_p - \omega_s)$ where ω_v is the Raman transition frequency. $\beta = \frac{\Gamma c \alpha}{16\pi}$ is a constant where c is the speed of light and α is the plane wave gain coefficient. Q is the coherent Raman polarization oscillating at the frequency ω_v. The nondepleted pump approximation is made throughout the work done in this thesis. This approximation sets $\frac{\partial}{\partial z}E_p = 0$.

The correspondence between the wave equation and the coupled differential equations which describe stimulated Raman scattering is straight forward to see.

Equation B.3 is solved for Q^* in the steady state approximation ($\frac{\partial Q^*}{\partial \tau} = 0$) and then substituted into equation B.2. This yields the equation

$$\frac{\partial E_s}{\partial z} = \beta \frac{\Gamma - i\Delta}{\Gamma^2 + \Delta^2} |E_p|^2 E_s \qquad \text{B.4}$$

The transverse lapacian is added to Eq.B.4 to account for diffraction of the Stokes beam. This term does not show up in the coupled differential equations because the coupled differential equations describe plane wave propagation.

APPENDIX C

THE NONLINEAR RAMAN SUSCEPTIBILITY

The non linear Raman susceptibility in vibrational Raman scattering in H_2 results from an induced dipole moment of the H_2 molecule due to the beating of the pump and Stokes fields[1]. In this case we will let the vibrational frequency, ω_v, of the H_2 molecule define the Raman resonance. For the beating of the pump and Stokes field to drive the induced dipole moment of the H_2 molecule, the difference between the pump and Stokes frequencies must be approximately equal to the resonant frequency of the H_2 molecule, $\omega_v \approx \omega_p - \omega_s$.

The vibrating H_2 molecule is modeled as a damped driven harmonic oscillator with a resonant frequency ω_v that satisfies the equation[1]

$$\frac{d^2}{dt^2}X(z,t)+\gamma\frac{d}{dt}X(z,t)+\omega_v^2X(z,t)=\frac{F(z,t)}{m} \qquad \text{C.1}$$

where X(z,t) is the vibrational coordinate, γ is a damping constant and is related to the collisional dephasing, Γ by the relationship $\Gamma = \gamma / 2$, m is the reduced mass of the H_2 molecule, and F(z,t) is the driving term.

The mechanism which is doing the driving is the beating of the pump and Stokes fields. Starting from the electric potential energy, an understanding of how the beating of the pump and Stokes fields can drive the H_2 molecule is found. The electric potential energy density is $u = \frac{1}{8\pi}\varepsilon|E|^2$ where ε is the electric permitivity and E is the total electric field. The electric permitivity can be written as[1]

$$\varepsilon = 1 + 4\pi N(\alpha_0 + \left.\frac{\partial \alpha}{\partial X}\right|_0 X(z,t) + \ldots) \qquad \text{C.2}$$

where a Taylor series expansion has been used for the molecular polarization α and N is the number density of H_2 molecules. Inplicit in this expansion is the steady state aprroximation. The potential energy and force are related by a derivative and the force per molecule can be written $F(z,t) = \frac{1}{N}\frac{\partial u}{\partial X} = \frac{1}{2}\left.\frac{\partial \alpha}{\partial X}\right|_0 |E|^2$. The total electric field contains both the pump and Stokes fields and is written

$E = \frac{1}{2}E_p(z)e^{i\omega_p t} + \frac{1}{2}E_s(z)e^{i\omega_s t} + c.c.$ where c.c. stands for the complex conjugate and will be used throughout this appendix. The driving force can now be written

$$F(z,t) = \frac{1}{8}\left.\frac{\partial \alpha}{\partial X}\right|_o \left[E_s^* E_p e^{i(\omega_p - \omega_s)t} + c.c\right] \qquad \text{C.3}$$

Only the terms which oscillate near the resonant frequency of the H_2 molecule are kept in the equation for the driving force. This approximation can be made because the H_2 molecule will react only near its resonant frequency $\omega_v \approx \omega_p - \omega_s$ and not to the other driving frequencies which result from $|E|^2$.

The equation of motion (Eq.C.1) can be solved by assuming a solution of the form $X(z,t) = \frac{1}{2} X(z) e^{i\omega t} + c.c.$. Using this ansatz, Eq.C.1, and Eq.C.3, one finds $\omega = \omega_p - \omega_s$ and

$$X(z) = \frac{1}{4m} \frac{\partial \alpha}{\partial X}\bigg|_0 \frac{E_s^* E_p e^{i(\omega_p - \omega_s)t}}{\omega_v^2 - (\omega_p - \omega_s)^2 + i\gamma(\omega_p - \omega_s)} + c.c. \qquad \text{C.4}$$

The polarization can be written with the aid of Eq.C.2 as

$$P = \varepsilon E_s = (1 + 4\pi N \alpha_0) E_s + 4\pi N \frac{\partial \alpha}{\partial X}\bigg|_0 X(z) E_s = P_L + P_{NL} \qquad \text{C.5}$$

where

$$P_L = (1 + 4\pi N \alpha_0) E_s$$

$$P_{NL} = 4\pi N \frac{\partial \alpha}{\partial X}\bigg|_0 X(z) E_s \qquad \text{C.6}$$

The non linear polarization $P_{NL} = N \frac{\partial \alpha}{\partial X}\bigg|_0 X(z) E_s$, can be written with the aid of Eq.C.4 as

$$P_{NL}(z,t)=\frac{N}{8m}\left(\left.\frac{\partial\alpha}{\partial X}\right|_0\right)^2\frac{\left|E_p\right|^2}{\omega_v^2-(\omega_p-\omega_s)^2+i\gamma(\omega_p-\omega_s)}\frac{1}{2}E_s e^{i\omega_s t}+c.c. \qquad \text{C.7}$$

A Stokes photon is emitted when the polarization oscillates at ω_s and it is for this reason that only the terms which oscillate at ω_s are kept in the above equation. Writing the non linear polarization as $P_{NL}(z,t)=\frac{1}{2}P_{NL}(z)e^{i\omega_s t}+c.c.$ allows use to write

$$P_{NL}(z)=\frac{N}{8m}\left(\left.\frac{\partial\alpha}{\partial X}\right|_0\right)^2\frac{\left|E_p\right|^2}{\omega_v^2-(\omega_p-\omega_s)^2+i\gamma(\omega_p-\omega_s)}E_s \qquad \text{C.8}$$

Using the relationship $P_{NL}(z)=\chi_{NL}\left|E_p\right|^2E_s$ and defining the Raman susceptibility as

$$\chi_R=\chi_{NL}\left|E_p\right|^2 \qquad \text{C.9}$$

one can write the Raman susceptibility from Eq.C.8 and Eq.C.9 as

$$\chi_R=\frac{N\left(\left.\frac{\partial\alpha}{\partial X}\right|_0\right)^2}{16m\omega_v}\left(\frac{\Delta\left|E_p\right|^2}{\Delta^2+\frac{\gamma^2}{4}}+i\frac{\frac{\gamma}{2}\left|E_p\right|^2}{\Delta^2+\frac{\gamma^2}{4}}\right) \qquad \text{C.10}$$

where the substitution $\Delta = \omega_v - (\omega_p - \omega_s)$ has been used. Δ is the detuning and tells how far away from the Raman resonance the pump and input Stokes are.

APPENDIX D

THE GAUSS-LAGUERRE MODES

The Gauss-Laguerre modes are the solution to the wave equation in free space which is written using the slowly varying envelope approximation as

$$\nabla_T^2 E(z, r_T) - 2ik\frac{\partial E(z, r_T)}{\partial z} = 0 \qquad \text{D.1}$$

where $E(z,r_T)$ is the slowly varying envelope of the electric field. Because the Gauss-Laguerre modes solve the wave equation, they are also known as the modes of free space. The Gauss-Laguerre modes are commonly used in optics and the solution to equation D.1 is available in the literature. The Gauss-Laguerre modes are written in cylindrical coordinates as

$$U_p^l(r,\varphi,z) = \frac{1}{\omega}\left[\frac{2p!}{\pi(l+p)!}\right]^{1/2}\left[\frac{\sqrt{2}r}{\omega}\right]^l L_p^l\left[\frac{2r^2}{\omega^2}\right] e^{-\frac{r^2}{\omega^2} - i\left[\pm l\varphi + \frac{kr^2}{2R} - (2p+l+1)\tan^{-1}(z/z_0)\right]} \qquad \text{D.2}$$

where p is the radial indice and l is the angular indice as will be seen in the figures, ω is defined as the spot size, k is the wavevector, z_0 is the Rayleigh range, L_p^l are the associated Laguerre polynomials, and R is the phasefront radius given by

$$R = z_0\left[(z/z_0) + (z_0/z)\right] \qquad \text{D.3}$$

The Gauss-Laguerre modes are directly used in the Gauss-Laguerre modal expansion and are indirectly used to make up the nonorthogonal modes. A understanding of what some of the lower order modes look like help give a physical feel for the modal solutions of the wave equation based on the Gauss-Laguerre modes.

Figure D1 shows the lowest order or U_0^0 mode. This mode is a focused gaussian and is used to describe the gaussian input Stokes signal into the Raman amplifier. Figure D2 is the U_2^0 mode. This mode still has rotational symmetry but the radial structure has change from that of the U_0^0 mode. Fig D3 is the U_0^2 mode. Notice the only the angular structure has change from the U_0^0 mode. Finally, figure D4 is the U_2^2 mode.

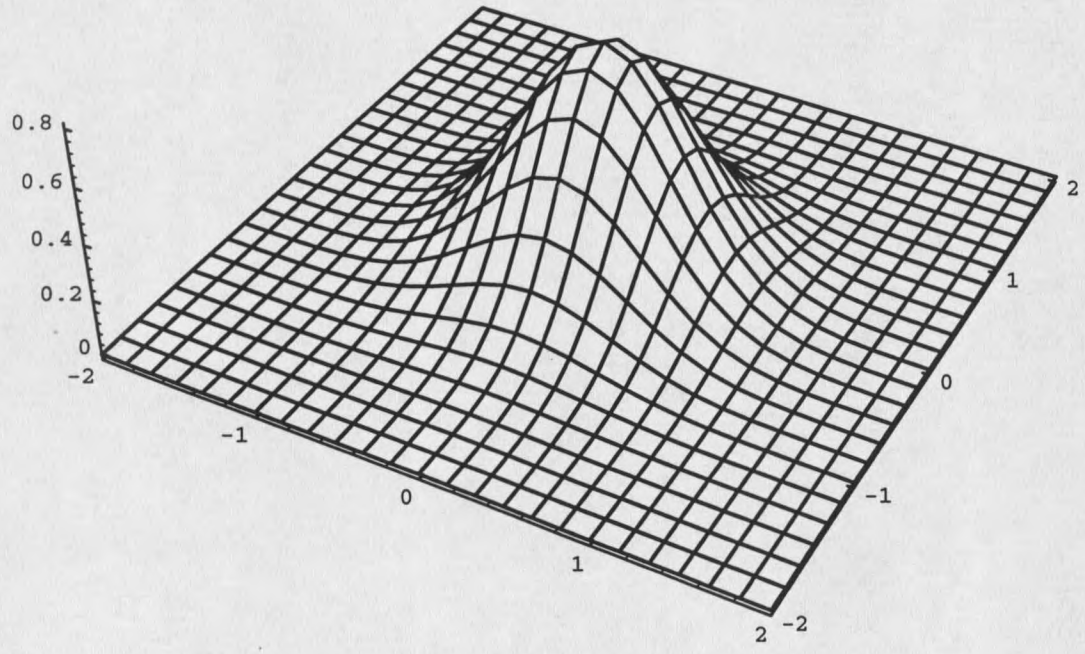


Figure D1 The U_0^0 Gauss-Laguerre mode. This mode is used to describe a focused gaussian beam.

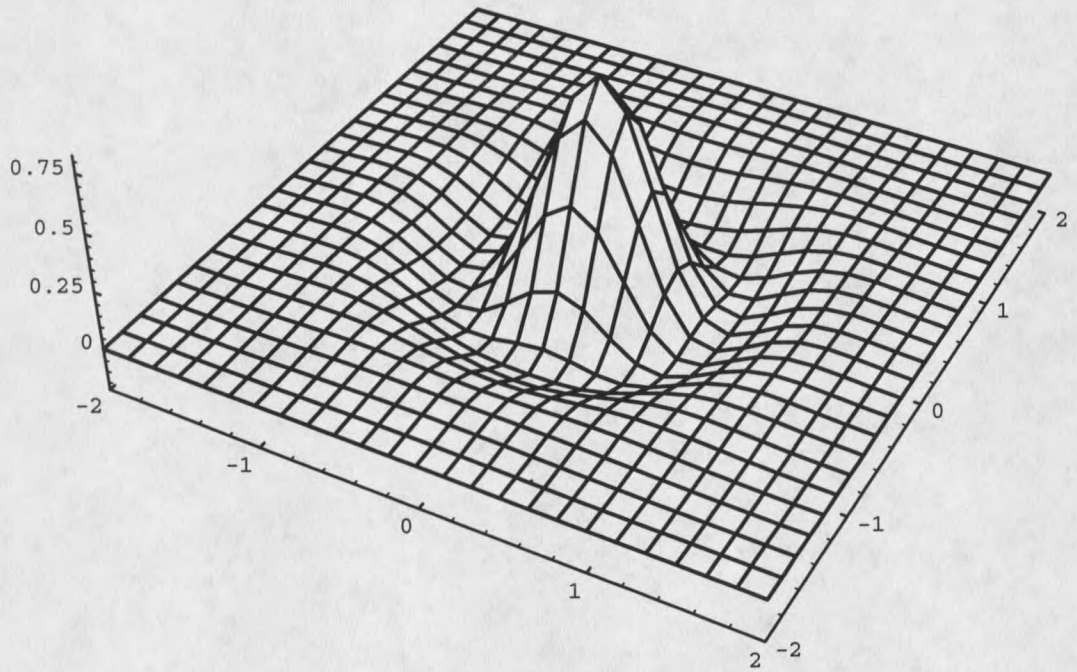


Figure D2 The U_2^0 Gauss-Laguerre mode. The p indice referres to the radial structure of the mode.

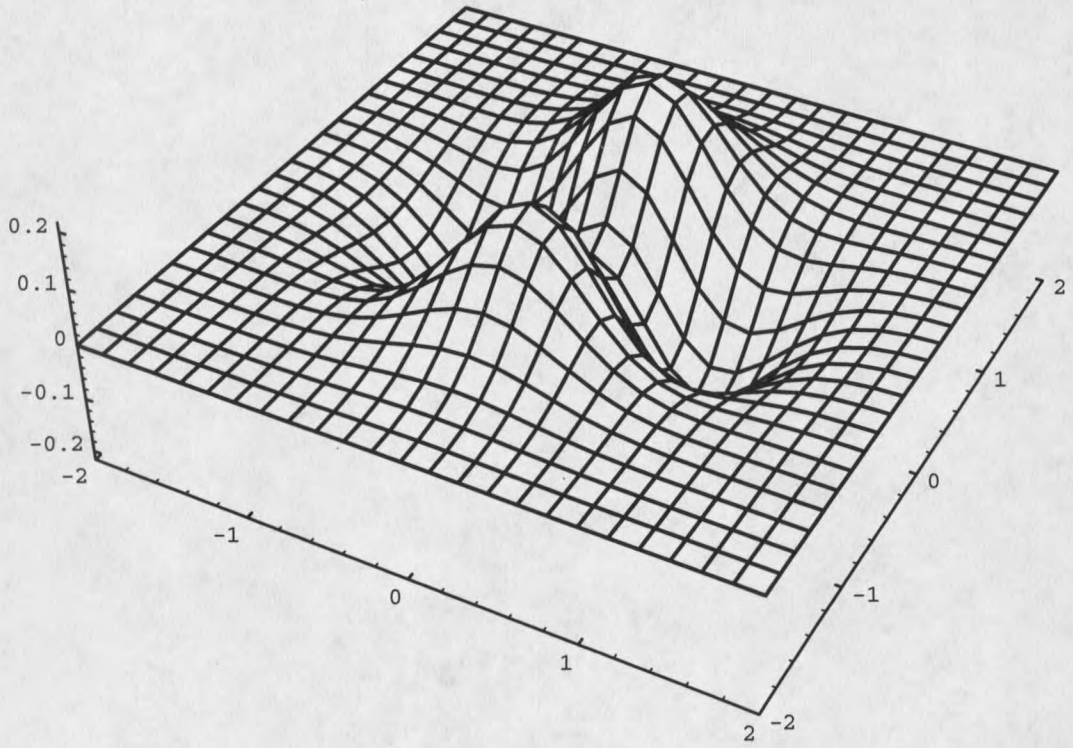


Figure D3 The U_0^2 Gauss-Laguerre mode. The l indice referres to the angular structure of the mode.

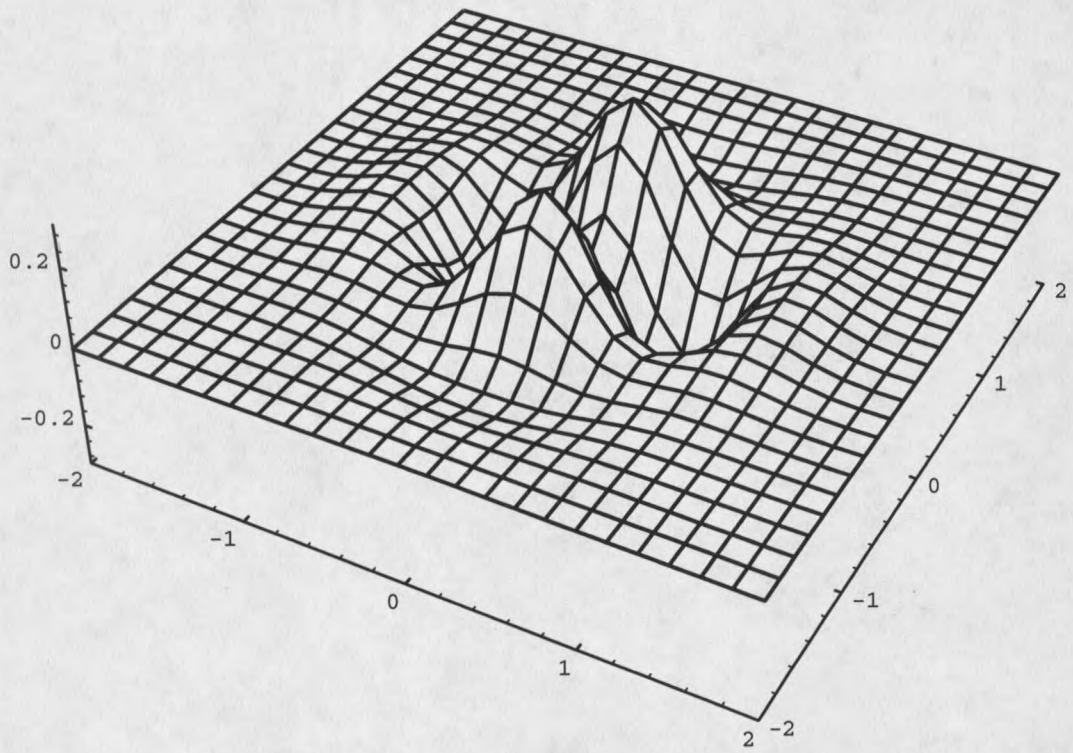


Figure D4 The U_2^2 Gauss-Laguerre mode.

APPENDIX E

THE $A^{l}_{p',p}(\mu, G; \theta, \theta_{in})$ MATRIX ELEMENTS

In this appendix the method used to calculate the matrix elements $A^{l}_{p',p}(\mu, G; \theta, \theta_{in})$ is given. Since the gain will not couple different l values, l is simply a parameter in the following equations. The matrix elements of $A^{l}_{p',p}(\mu, G; \theta, \theta_{in})$ are found from the matrix $A(\mu, G; \theta, \theta_{in})$ which is formed by

$$A(\mu, G; \theta, \theta_{in}) = U^{+}(\theta) S e^{D(\theta-\theta_{in})} S^{-1} U(\theta_{in}) \qquad \text{E.1}$$

where the matrix elements of U are defined by

$$U^{l}_{p',p}(\theta) = \left(e^{iH\theta}\right)^{l}_{p',p} \qquad \text{E.2}$$

and the matrix elements of H are given by

$$H^{l}_{p',p} = 2p\delta_{p',p} \qquad \text{E.3}$$

Also needed in Eq.E.1 are the matrices D and S. These matrices are found by diagonalizing the matrix K+iH such that

$$S^{-1}(K + iH)S = D \qquad \text{E.4}$$

where the matrix elements of H are given by equation E.3 and the matrix elements of the matrix K are given by

$$K^{l}_{p',p} = \mu G Q^{l}_{p',p}(\mu) \qquad \text{E.5}$$

where G is the gain and $Q^{l}_{p',p}$ is defined in below.

The $Q^{l}_{p',p}(\mu)$ is a complex polynomial that has been given in the literature. For sake of completeness it is repeated here. The $Q^{l}_{p',p}(\mu)$ polynomial is in general terms written $Q^{s}_{h,q}$ where h≥q as

$$Q^{s}_{h,q} = \mu^{s}\left[\frac{h!q!}{(h+s)!(q+s)!}\right]^{1/2}\sum_{m=0}^{q}\binom{q+s}{m}\binom{h+s}{m+h-q}\frac{(q-m+s)!}{(q-m)!}\mu^{2(q-m)}(1-\mu)^{2m+h-q} \qquad \text{E.6}$$

APPENDIX F

MODE MATCHING AND ALIGNMENT OF THE HIGH FINESSE INTERFEROMETER

The nonconfocal cavity of the HFI is constructed of two spherical mirrors of radius R_m separated by a distance d with $d<<R_m$. In general the electric field inside the cavity is expressed as an infinite set of spatial modes. However, the HFI is most useful when only one of the modes, usually the lowest order or fundamental mode , is excited. Care must be taken when setting up an HFI so that the higher order spatial modes can be suppressed. The higher order spatial modes will be suppressed when the HFI cavity is mode matched. In the simplest sense, mode matching means providing the cavity with the input beam whose phasefronts exactly match the mirror curvature. The input beam phasefronts will match the mirror curvature when the input beam Rayleigh range matches the Rayleigh range of the nonconfocal cavity.

The Rayleigh range of the HFI, denoted by z_{0c}, is given by

$$z_{0c} = \tfrac{1}{2}\left[d(2R_m - d)\right]^{1/2} \qquad \text{F.1}$$

where d is the length of the cavity and R_m is the radius of curvature of the mirrors. Figure F1 shows a simplified experimental set up that will allow the Rayleigh range of the input beam to match the Rayleigh range of the HFI cavity. The input beam will be centered in the HFI and have the same Rayleigh range as the HFI when d_1, d_2, and f are chosen such that the following two equations are satisfied

$$z_{oc} = \frac{z_{0f} f^2}{(f - d_1)^2 + z_{of}^2} \qquad \text{F.2}$$

$$d_2 = \frac{z_{0f}^2 f + d_1^2 f - d_1 f^2}{(f - d_1)^2 + z_{0f}^2} \qquad \text{F.3}$$

where z_{of} is the Rayleigh range of the light that is exiting the fiber, f is the focal length of the lens shown in figure F1, d_1 and d_2 are shown in figure F1, and z_{0c} is the Rayleigh range of the HFI cavity given by equation F.2.

Alignment of the cavity involves launching the input beam along the cavity axis with the beam waist at the center of the cavity. The waist needs to be approximately within 100 μm of the center of the cavity, and the input needs to be within approximately 2mrad of the cavity axis to be aligned. Figure F2 shows the apparatus setup used to align the HFI. The HFI is positioned in the beam so that the mirrors are approximately centered on the waist. The HFI is held in a mount that allows both angle and position adjustments in the horizontal and vertical directions. A back reflection from the front mirror of the cavity is adjusted to overlap the input beam. This will roughly align the HFI. Once the cavity is roughly aligned and mode matched, finer adjustments can be made. The mirror in figure F2 is mounted on a kinematic mount to allow viewing of the output beam with either a camera or photodiode.

In figure F3a the cavity is poorly aligned. As the vertical and horizontal tilts are adjusted the cavity comes into better alignment. Figure F3b shows the intensity pattern

starting to collapse in the video image. The fundamental mode is starting to appear as the left hand peak in the oscilloscope. As the cavity is adjusted more, the intensity pattern continues to collapse, and the fundamental mode becomes more dominant. This is shown in figure F3c. Finally in figure F3d a well matched cavity is shown. Note the circular pattern of the video image and the single strongly peaked mode on the oscilloscope.

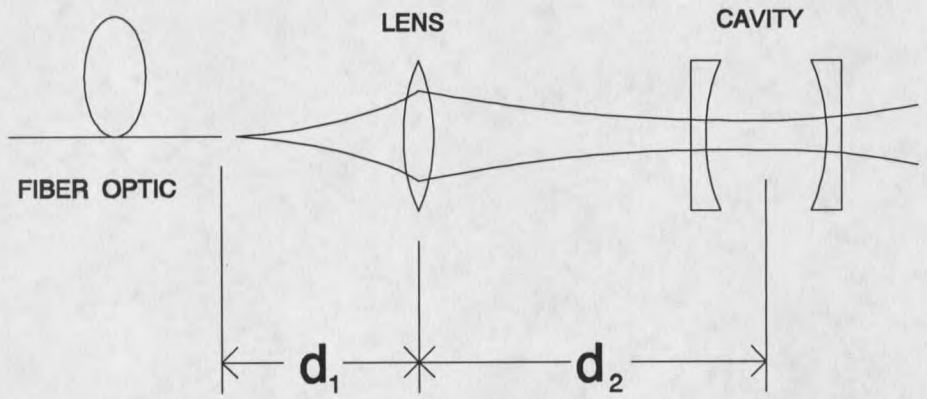


Figure F1 Experimental setup for mode matching the input beam with the HFI.

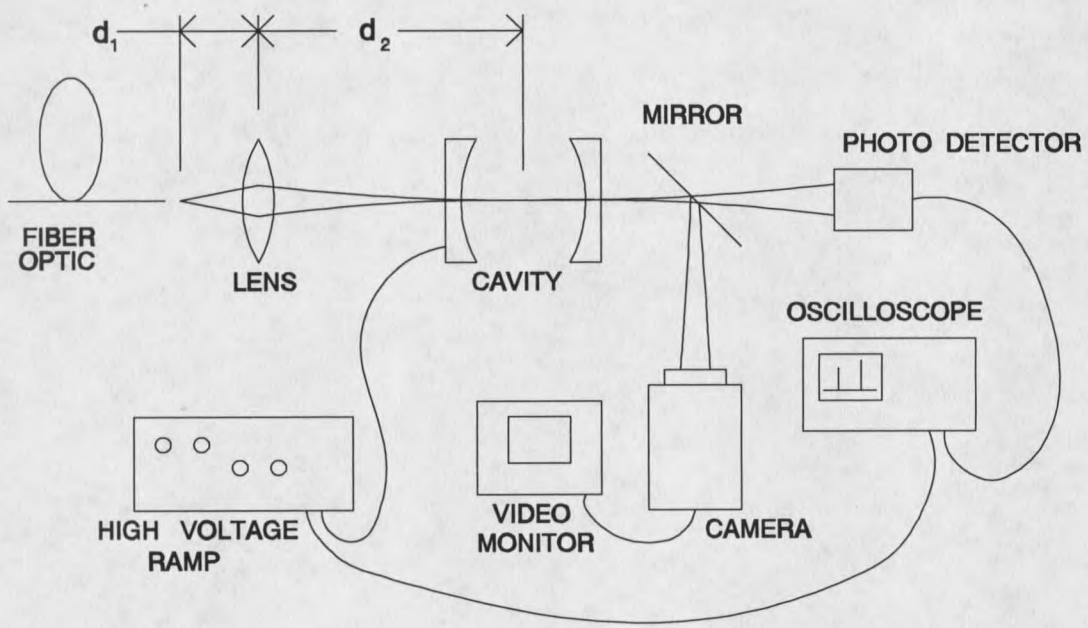
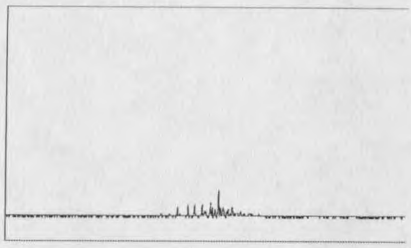
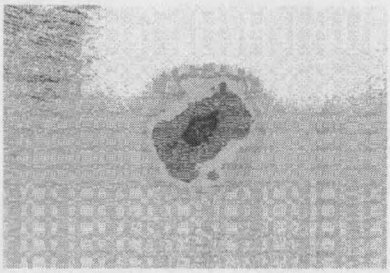


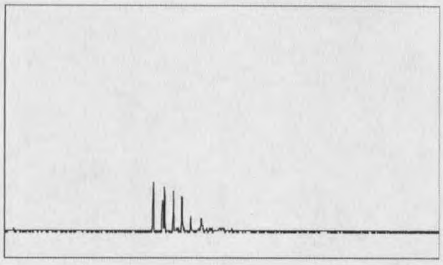
Figure F2 Experimental apparatus used to align the HFI. The fiber optic and lens are held in a fiber coupler.





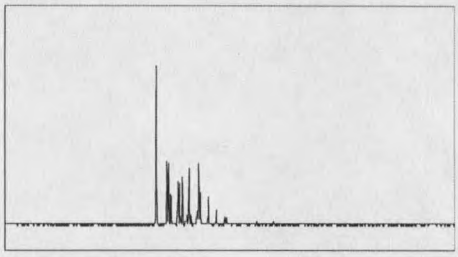
D3(a)



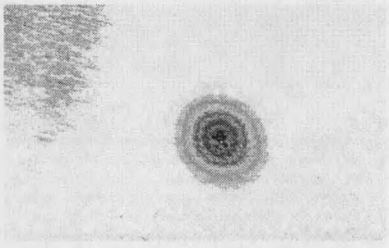


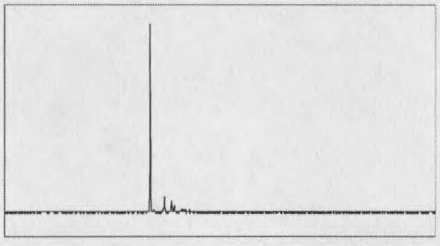
D3(b)





D3(c)





D3(d)

Figure F3 Video image and corresponding oscilloscope trace showing the mode structure at various stages of alignment.

APPENDIX G

RAMAN LINEWIDTH

The Raman linewidth Γ is a critical parameter used throughout this thesis. An accurate value of Γ is crucial for comparing the theoretical and experimental results in this thesis. The Raman linewidth is presented in the literature and in this appendix we experimentally confirm the predictions of the literature and provide an accurate method to experimentally measure Γ.

The experimental setup which allows us to measure the Raman linewidth as a function of the pressure of the H_2 is the same as in figure 23. However in this experiment the pump energy is kept high so that the PMT is not needed. Data is collected as follows. The TLD is swept across the Raman linewidth and the pump energy, relative input Stokes frequency, and output Stokes energy is recorded for each shot of the pump laser. Twelve hundred points were collected at each pressure and then the pressure of the H_2 was changed and another twelve hundred data points taken.

The data was fitted to

$$E_s(out) = E_s(in)e^{-gz\frac{\omega^2}{\omega^2+\Gamma^2}} \qquad \text{G.1}$$

where E_s(out) is the measured output Stokes energy, E_s(in) is the input Stokes energy, gz is related to the gain G, and ω is the Stokes frequency using a least squares fit to find a value for the Raman linewidth. The results are shown in figure G1. The +'s are experimental values and the solid line is the theoretical predictions. The experimental values match the theoretical predictions.

The Raman linewidths for the experiments were measured this way and the results of this measurement were used in the calculations.

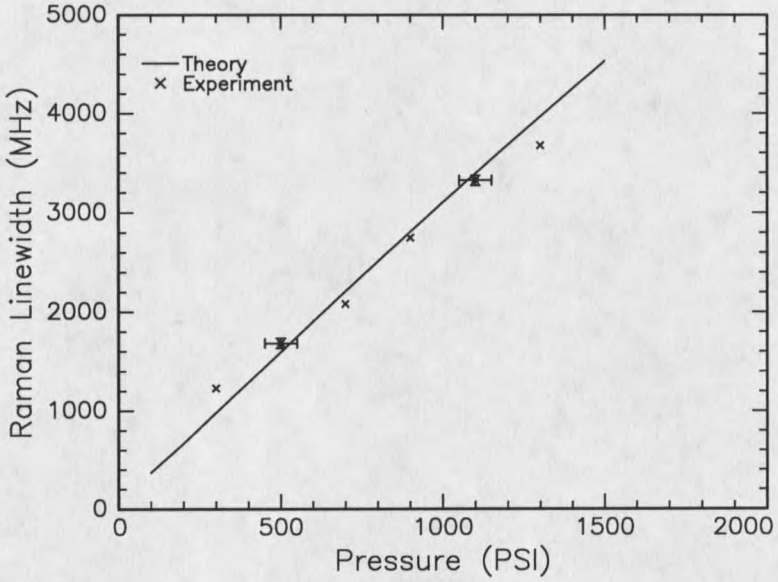


Figure G1 Plot of the linewidth, Γ, as a function of the cell pressure. The solid line is the predicted value of the Raman linewidth from Ref.31. The +'s are experimentally measured values of the Raman linewidth.

MONTANA STATE UNIVERSITY LIBRARIES
3 1762 10235804 9